NAVWEPS REPORT 7655
NOTS TP 2680
COPY 94

PERFORMANCE CHARACTERISTICS OF AN INTERMITTENT-DETONATION DEVICE

by

L. J. Krzycki
Propulsion Development Department

ABSTRACT. An analytical and experimental investigation was conducted to determine the operating characteristics of an intermittent-combustion device employing gaseous detonative combustion. Gaseous propane and air were used as propellants in the experimental investigation.

Results indicated that the intermittent-detonation device was capable of operating on at least two "resonant" spark-energization frequencies. For the device used in the investigation these frequencies were approximately 25 and 50 cps. Reaction thrust, noise output, and actual combustion frequency were noticeably greater at the resonant conditions than at other operating points.

Reloading the tube with fresh charge occupied most of the cycle time, which limits the operating frequency of the device. The device does not appear promising as a thrust producing mechanism because of its low operating frequencies.

U. S. NAVAL ORDNANCE TEST STATION
China Lake, California
June 1962

U. S. NAVAL ORDNANCE TEST STATION

AN ACTIVITY OF THE BUREAU OF NAVAL WEAPONS

C. BLENMAN, JR., CAPT., USN
Commander

WM. B. McLEAN, PH.D.
Technical Director

FOREWORD

This work is part of a continuing study of detonation being conducted at the U. S. Naval Ordnance Test Station. The experimental work, carried out between January and June 1960, was supported by BuWeps Task Assignment NO-505736-63087-01060 and applied research funds.

The information in this report was presented as a thesis in partial fulfillment of the requirements for the degree of Master of Science. As such, it was reviewed for technical accuracy by J. M. F. Vickers of the University of Nebraska.

Released by
H. POWELL JENKINS, *Head,*
Propulsion Applied Research Group
8 March 1962

Under authority of
J. T. BARTLING, *Head,*
Propulsion Development Dept.

NOTS Technical Publication 2680
NAVWEPS Report 7655

Published by ..... Publishing Division
Technical Information Department
Supersedes ..... IDP 1077
Collation ..... Cover, 26 leaves, abstract cards
First printing .....165 numbered copies
Security classification .....UNCLASSIFIED

INITIAL DISTRIBUTION

28 Chief, Bureau of Naval Weapons

CS (1)	RAAV-34 (1)	RMMP-24 (1)
DLI-31 (2)	RAPP (1)	RMMP-33 (1)
DMP-33 (1)	RM (1)	RMMP-4 (1)
FWAM (1)	RM-1 (1)	RMMP-42 (1)
FWWS-3 (1)	RM-3 (1)	RRMA-221 (1)
P-1 (1)	RM-35 (1)	RRRE (1)
PMA-3 (1)	RMMP (1)	RRRE-5 (1)
R-12 (1)	RMMP-12 (1)	RT (1)
R-5 (1)	RMMP-2 (1)	RUME-11 (1)

5 Chief of Naval Operations
- Deputy Chief for Air (1)
- Operations Evaluation Group (1)

2 Chief of Naval Research
- Code 104 (1)
- Code 463 (1)

1 Assistant Secretary of the Navy (Material) (Mr. Moore)
1 Fleet Anti-Air Warfare Training Center, San Diego (Guided Missile Section)
1 Naval Air Force, Atlantic Fleet
1 Naval Air Force, Pacific Fleet
1 Naval Air Material Center, Philadelphia
1 Naval Air Test Center, Patuxent River (Aeronautical Publications Library)
1 Naval Avionics Facility, Indianapolis (Library)
1 Naval Ordnance Laboratory, White Oak (Library)
2 Naval Propellant Plant, Indian Head
1 Naval Research Laboratory (Code 2021)
2 Naval Underwater Ordnance Station, Newport
1 Naval Weapons Laboratory, Dahlgren (Technical Library)
2 Naval Weapons Services Office, Naval Weapons Plant
1 Operational Test and Evaluation Force
1 Bureau of Naval Weapons Fleet Readiness Representative Pacific, Naval Air Station, North Island
1 Bureau of Naval Weapons Representative, Azusa, Calif.
4 Chief of Ordnance
- ORDTA (1)
- ORDTB (1)
- ORDTS (1)
- ORDTU (1)

2 Aberdeen Proving Ground
- Ballistic Research Laboratories (1)
- Development and Proof Services (1)

7 Army Rocket and Guided Missile Agency, Redstone Arsenal
  ABMA (1)
  ORDDW-IDE (1)
  ORDXR-ODA (1)
  ORDXR-OTL, Technical Library (4)
1 Diamond Ordnance Fuze Laboratory (Library)
2 Frankford Arsenal
  ORDBA-1421 (1)
  Pitman Dunn Laboratory (1)
1 Picatinny Arsenal (Library)
1 Rock Island Arsenal
3 White Sands Missile Range (Library)
1 Headquarters, U. S. Air Force (AFDRD-CC)
1 Aeronautical Systems Division, Wright-Patterson Air Force Base (ASAPRD-Dist)
1 Air Force Cambridge Research Laboratories, Laurence G. Hanscom Field
1 Air Proving Ground Center, Eglin Air Force Base (PGEM)
1 Air University Library, Maxwell Air Force Base
1 Holloman Air Force Base
2 Ogden Air Materiel Area, Hill Air Force Base (OORE)
1 Tactical Air Command, Langley Air Force Base (TPL-RQD-M)
1 Advanced Research Projects Agency
10 Armed Services Technical Information Agency (TIPCR)
1 Weapons Systems Evaluation Group
1 Aerojet-General Corporation, Azusa, Calif. (Librarian) via BuWepsRep
1 Aerojet-General Corporation, Sacramento (Librarian) via BuWepsRRep
1 Allegany Ballistics Laboratory, Cumberland, Md.
2 Applied Physics Laboratory, JHU, Silver Spring
1 Atlantic Research Corporation, Alexandria, Va.
1 Continental Aviation and Engineering Corporation, Detroit (Librarian)
1 Experiment, Inc., Richmond, Va.
1 Institute for Defense Analyses
1 Jet Propulsion Laboratory, CIT, Pasadena (Dr. W. H. Pickering)
1 Research Analysis Corporation, Bethesda, Md. (Document Control Office)
1 University of Chicago, Institute for Air Weapons Research (Library)

CONTENTS

ACKNOWLEDGMENT

The author wishes to thank the following members of the University of Nebraska faculty and staff: J. M. F. Vickers, under whose guidance and encouragement the project was initiated; J. W. Harper, for his advice in apparatus design and assistance in securing equipment; R. H. Joosten and C. D. Mittan, for assistance in apparatus construction; and N. H. Barnard, Chairman of the Mechanical Engineering Department, for the use of facilities.

At the U. S. Naval Ordnance Test Station, the author wishes to thank H. Powell Jenkins, Jr., for the use of facilities and C. L. Spindler for advice and criticism.

NOMENCLATURE

A	Area, ft^2
a	Speed of sound, ft/sec
$\bar{a}$	a/a_0, dimensionless form of a
B	Constant, ft/lb
C	Constant, ft/lb
F	Instantaneous thrust, lb
f	Frequency of spark energization, cps
F_{av}	Average thrust, lb
I_{sp}	Specific impulse, lb thrust/lb fuel/sec
L	Length, ft
M	Mach number, V/a
m	Molecular weight
P	$\frac{2}{\gamma - 1}\bar{a} + U$, Riemann variables
p	Static pressure, lb/ft^2
Q	$\frac{2}{\gamma - 1}\bar{a} - U$, Riemann variables
R	Gas constant, ft-lb/lb-°R
S	$\frac{s}{C_p(\gamma - 1)}$, dimensionless form of s
s	Specific entropy, Btu/lb °R
T	Absolute static temperature, °R
t	Time, sec
$U + \bar{a}$	Slope of P Riemann variable
$U + \bar{a}$	Slope of Q Riemann variable
u	Flow velocity relative to duct, ft/sec
U	u/a_0, dimensionless form of u
V	Average velocity with reference to duct, ft/sec
v	Shock velocity relative to duct, ft/sec
W	v/a_0, dimensionless form of v
w	Weight flow of fluid, lb/sec
x	Distance, ft

α Injection angle, degrees

γ Ratio of specific heats, c_p/c_v

θ Air–fuel ratio, (lb-air/sec)/(lb-fuel/sec)

ξ x/L_0, dimensionless form of x

ρ Density, lb/ft^3

τ $a_0 t/L_0$, dimensionless form of t

SUBSCRIPTS

0 Initial conditions, reference to atmosphere

1 Conditions in unburned gas

2 Conditions in burned gas behind detonation wave

3 Conditions in burned gas behind trailing rarefaction wave

2c Conditions in burned gas relative to tube

a Air

av Average

c Cycle

d Detonation

ex Exhaust

f Fuel

i Conditions at injection plane

m Mixture

INTRODUCTION

Under certain conditions of pressure, volume, and composition of various combustible gas mixtures in tubes, a flame front will propagate through the mixture at speeds ranging from 3,000 to 12,000 ft/sec upon ignition of the mixture. This front is called a detonation wave and the propagating speed is the detonation velocity. Much experimental and theoretical work has been devoted to the study of detonation waves, mainly in shock tubes in which the wave is in a transient state. Until recently, however, little work had been done from the viewpoint of utilizing the energy associated with these supersonic combustion waves. The relatively high pressures associated with detonative combustion could conceivably be used in a reaction propulsion device.

Detonative combustion can be applied to a reaction engine in three ways.

1. Accelerate a combustible gas at high total temperature and pressure to the local detonation velocity (3,000–12,000 ft/sec) and then cause it to ignite, thus establishing a standing (steady-state) detonation wave.

2. Stabilize a detonation wave near the exit section of a convergent–divergent nozzle (rocket motor), so that advantage may be taken of very-high-energy fuels using normal combustion-chamber materials and normal cooling techniques.

3. Operate intermittently in the manner of a pulse jet, but utilize the supersonic combustion properties of the detonation wave.

This investigation is concerned with the performance characteristics of an intermittent-detonation device using propane–air mixtures. Idealized relationships among the physical parameters of the detonation device, the air–fuel ratio, the air flow rate, and the frequency of spark energization have been derived from basic fluid-flow equations, and experiments have been performed to verify these equations.

The intermittent-detonation device was operated with propane–air mixtures in preliminary runs at the University of Nebraska in February, 1959. Experimental results reported here were obtained at the U. S. Naval Ordnance Test Station.

LITERATURE REVIEW

In the latter part of the nineteenth century, the French physicists Berthelot and Vieille (Ref. 1) and Mallard and LeChatelier (Ref. 2) found that in a combustible mixture under certain conditions, combustion waves developed that possessed propagation velocities considerably greater than the velocity of sound at ordinary temperatures and pressures. Chapman (Ref. 3), Jouguet (Ref. 4), and Dixon (Ref. 5) independently advanced the explanation that the steady-state detonation that is commonly observed in experiments has a fluid flow immediately behind the detonation wave with a Mach number exactly equal to one relative to the wave. Such a detonation wave is called a Chapman-Jouguet detonation. Von Neumann (Ref. 6), Doring (Ref. 7), and Zeldovitch (Ref. 8) independently analyzed the problem of the internal conditions in the detonation wave. The detonation wave was considered to be composed of a normal shock followed by a deflagration.

The deflagration was thought to be initiated by a temperature increase across the shock wave. Recent photographic studies by Greifer et al (Ref. 9) tend to confirm this explanation. The Von Neumann (Ref. 6) model of a detonation wave is based on the assumption that viscous dissipation, heat conduction, and diffusion effects may be neglected, in first approximation, in the description of wave structure. Hirshfelder and Curtiss (Ref. 10) have investigated the internal conditions of a detonation wave with simplifying assumptions about the chemical kinetics, but including the effects of viscosity, diffusion, and thermal conductivity.

Experiments by Turin and Huebler (Ref. 11) and Shckelkin (Ref. 12) tend to support the theory that both wave phenomena and turbulence account for the transition and that it is controlled by one or the other or both, depending on the physical characteristics of the combustion tube. Morrison (Ref. 13) has shown that the Mach number of detonation is an important parameter in detonation phenomena.

The first reported work on intermittent detonation was done by Hoffmann (Ref. 14) in 1940. He operated an intermittent-detonation device successfully with acetylene–oxygen mixtures by using water vapor to prohibit premature burning, and with liquid fuels, namely benzine–oxygen mixtures. Hoffmann measured thrust for various operating conditions, and found that the distance from the fuel injector to the spark source and the length of the diffuser beyond the spark source were important factors.

The next work was reported by Nicholls, Wilkinson, and Morrison (Ref. 15) in 1955. They operated an intermittent-detonation device with hydrogen–air mixtures. For a constant fuel–air ratio and a given air flow rate it was found that the thrust increased to a maximum and then decreased with increasing frequency of detonation. The measured specific impulse was in good agreement with that predicted by their simplified wave analysis in which experimental values of the detonation velocity for hydrogen–air mixtures were used.

THEORY

The physical characteristics of the intermittent-detonation device are such that it may be compared readily with the classical experimental apparatus used for the observation of gaseous detonation waves. The classical tube is of circular cross section with much greater length than diameter and with one end closed. An ignition source is located near the closed end. The tube is filled with a gaseous combustible mixture, the mixture is ignited, and measurements and observations are made as the deflagration accelerates to a detonation and proceeds to the open end of the tube. A more thorough discussion of the transition from deflagration to detonation is given in Appendix A. Only one detonation is produced in the classical apparatus, and the tube must be recharged with unburned mixture after each firing. The intermittent-detonation device differs in that the closed end is replaced with a manifold system so that the combustion mixture is continually discharged into the tube. In addition, the spark ignition source is energized at a constant frequency rather than by the single pulse that is given to it in the classical detonation tube.

The specific impulse, I_{sp}, for an air-breathing reaction–propulsion device is defined as the thrust that would be obtained from an equivalent device that has a fuel-weight flow rate of unity. It is defined as

$$I_{sp} = \frac{F_{av}}{w_f}$$

where F_{av} is the average thrust in pounds, and w_f is the fuel-weight flow rate in lb/sec.

Considering the tube as a system and neglecting frictional losses, the only force acting on the tube is that due to the pressure unbalance on the closed end of the tube ($p_3 - p_1$). When a detonation wave is formed at the closed end of a tube, it is followed by a rarefaction wave that slightly reduces the high pressure immediately behind the detonation wave and also brings the gas behind the detonation wave to rest. The maximum instantaneous thrust, F, is given by

$$F = (p_3 - p_1)A = Ap_1\left(\frac{p_3}{p_1} - 1\right)$$

where p_1 is the pressure in the unburned mixture, p_3 is the pressure behind the trailing rarefaction wave, and A is the cross-sectional exhaust area of the tube. Morrison (Ref. 13) has shown that the pressure ratio p_3/p_1 is given by

$$\frac{p_3}{p_1} = \left(\frac{1 + \gamma_1 M_1^2}{1 + \gamma_2}\right)\left(1 - \frac{\gamma_2 - 1}{2} M_{2c}\right)^{2\gamma_2/(\gamma_2 - 1)} \tag{1}$$

where M_1 is the Mach number of detonation, M_{2c} is the Mach number of the burned gases with respect to the tube, γ is the ratio of specific heats, and the subscripts 1 and 2 refer to conditions in the unburned and burned gas, respectively.

For an intermittently operating device p_3 decreases during the exhaust time, t_{ex}, until atmospheric pressure is reached. Therefore, the thrust also decreases in this time interval. The average thrust for the cycle is given by

$$F_{av} = \left(\int_0^{t_{ex}} F dt\right)/t_c \tag{2}$$

where t_c is the time for one cycle. It includes

t_d, the time for the detonation wave to travel the tube length L

t_{ex}, the time for the tube to exhaust to atmospheric pressure

t_m, the time to introduce a fresh mixture charge.

An expression for the pressure on the closed end of the tube as a function of time must be determined before the average thrust given by Eq. 2 can be evaluated.

WAVE-MECHANISM ANALYSIS

The flow of burned gas from the detonation tube and the decay of pressure of the burned gas are phenomena complicated by the interaction of expansion, compression, and shock waves that propagate up and down the tube. The flow rate and pressure of the burned gas depend directly on the wave phenomena. The only analytical method of determining accurately this wave interaction is the method of characteristics. The wave diagram resulting from this graphical method represents the propagation of waves in space and time. Only specific problems can be solved by this method; no general solution of the problem of unsteady flow in ducts is known.

An analysis has been made of the wave phenomena occurring in the discharge of the detonation tube for a specific case. This analysis was made with the following simplifying assumptions that were necessary for the solution of the problem.

1. Flow is isentropic.

2. The Chapman-Jouguet detonation condition is established immediately at the closed end of the tube.

3. The detonation wave and trailing rarefaction wave travel as two waves separated by a negligible distance.

4. The detonation wave increases the pressure of the gas within the tube. The temperature of the burned gas then corresponds to that indicated by the isentropic boundary conditions.

5. A shift in the center of mass of the burned gas does not occur as the detonation wave proceeds to the open end of the tube.

6. The fresh mixture charge begins to flow into the closed end of the tube when atmospheric pressure is reached at the closed end.

7. The interface between the fresh charge and the burned gas is a discontinuity that moves at constant velocity determined by continuity considerations. Interface velocity can be altered only by shock–interface interactions.

8. There are no valving or frictional losses.

The most probable deviation from actual conditions will result from the assumption of isentropic temperature, which is a direct result of the original isentropic-flow assumption.

The wave diagram resulting from the method of characteristics solution is shown in Fig. 1. The computed values from which this diagram was drawn are tabulated in Table 1, together with the specific conditions for which the problem was solved. An explanation of the computing procedure is given in Appendix B. Reference 16 was used as the main source for computational procedure.

EXPLANATION OF WAVE DIAGRAM

The wave diagram (Fig. 1), is a dimensionless time–distance plot. The slope of the waves is an indication of their relative velocity. The flow phenomena may be explained as a number of discrete steps; the wave diagram begins with step 3.

1. Ignition of the combustible mixture results in a detonation wave and trailing rarefaction wave that propagate to the open end of the tube and increase the pressure of the gas within the tube.

2. The detonation wave reaches the open end of the tube and a shock of lesser strength is transmitted into the surrounding atmosphere. The burned gas within the tube is quiescent because of the action of the trailing rarefaction wave.

3. A centered expansion fan races back into the tube and accelerates the gas to a finite velocity. The exit velocity remains constant and sonic between points 0–9.

4. The reflected expansion waves, points 1–9 and 10–17, cannot be reflected back into the tube because of the sonic flow condition at the exit. Therefore, they simply move out of the end of the tube.

5. Flow at the exit remains sonic until the pressure is reduced to a point where subsonic flow can occur, and waves can be reflected back into the tube. This condition occurs between points 17 and 24. Therefore, when the reflected third wave of the expansion fan, points 18–24, reaches the open end of the tube, it is reflected as a compression wave.

6. The reflected third and fourth compression waves, points 18–24 and 25–31, merge to form a shock wave that moves toward the closed end of the tube.

7. The arrival and reflection of the original expansion fan at the closed end of the tube reduces the closed-end pressure until, at a point slightly above point 39, the pressure is atmospheric. At this point the charge of fresh mixture begins to flow into the tube at a constant velocity.

8. Crossing of the interface by the expansion waves at points 46 and 55 would probably result in transmitted waves into the fresh mixture. These have been neglected in this analysis. Because of their weakness, their probable effect on the fresh mixture would be negligible. Instead, the expansion waves are reflected from the interface and propagate toward the open end of the tube.

9. The weak shock propagating into the tube crosses the interface, and the weaker transmitted shock is reflected from the closed end of the tube and again crosses the interface. The result of these two crossings is, in each case, an expansion fan that accelerates the interface. However, these accelerations are in opposite directions and result in no appreciable change in the interface velocity.

10. A very weak shock is transmitted from the second shock–interface interaction and propagates toward the open end of the tube. When the shock arrives at the open end of the tube a centered expansion fan is originated that travels back into the tube.

The wave diagram was discontinued at this point because the wave interactions are now so weak that no appreciable effect results.

The movement of the interface drives the burned gas from the tube, and there is no inflow of atmospheric air into the open end of the tube. The pressure history at the closed end of the tube (Fig. 2) has been drawn from the pressure-ratio values obtained in the wave-diagram computations. The general shape of the pressure-decay curve will remain the same for various air–fuel ratios and air flow rates; however, the specific values of the time and pressure ratios will change. Thus, no general analytical expression is available for the determination of the pressure decay within the detonation tube. For the conditions of Fig. 1, the exhaust time is about 13.5 milliseconds.

The solution discussed above yields an exhaust time that is too long, because a low value was used for the speed of sound in the burned gas (based on an isentropic value obtained from the pressure ratio). The characteristics solution yields information about the nature of the expansion, compression, and shock waves to be expected within the duct, but does not give an accurate analysis of the magnitude of the physical quantities involved.

The simplified wave solution proposed in Ref. 15 assumed that the pressure in the burned gas was reduced to atmospheric by one returning rarefaction wave traveling at the sound velocity of the burned gas. This startling simplification is shown reasonable by the characteristics solution. Perhaps the strongest argument is that theoretical results compare surprisingly well with experimental results. The equations, arranged to include the air–fuel ratio, θ, can be expressed as

$$F_{av} = \frac{t_{ex}}{t_c} A p_1 \left[\left(\frac{1 + \gamma_1 M_1^2}{1 + \gamma_2} \right) \left(1 - \frac{\gamma_2 - 1}{2} M_{2c} \right)^{2\gamma_2/(\gamma_2 - 1)} - 1 \right] \tag{3}$$

and

$$I_{sp} = \frac{t_{ex} A p_1 \theta}{t_c W_a} \left[\left(\frac{1 + \gamma_1 M_1^2}{1 + \gamma_2} \right) \left(1 - \frac{\gamma_2 - 1}{2} M_{2c} \right)^{2\gamma_2/(\gamma_2 - 1)} - 1 \right] \tag{4}$$

Computations for Eq. 3 and 4 are tabulated in Table 2; plots of the equations are shown with experimental results in Fig. 28 and 29.

DETONATION-TUBE LOADING

Because of the semicontinuous operation of the intermittent-detonation device, the possibility exists that, above certain frequencies, the detonation wave may overrun the burned products of the previous cycle. This collision would result in a mild rarefaction wave reflected upstream and a shock wave transmitted downstream into the burned products, with a consequent loss of thrust. This has been reported in Ref. 15 for hydrogen–air mixtures. Therefore, for maximum specific impulse to be obtained from ideal mechanical operation of the detonation tube, the cycle should be repeated only when the tube has been completely refilled with unburned mixture. If the cycle is repeated at some time after the tube is completely refilled, a lower specific impulse will be realized because of the loss of fuel to the atmosphere.

The rate at which the unburned mixture fills the tube is controlled primarily by the air flow rate for a tube of constant cross section and length. Assuming incompressible flow, the flow velocity in the tube may be determined using

$$w_m = \rho_m A V_m$$

where w_m is the total mass flow rate, ρ_m is the mixture density, A is the tube exhaust area, and V_m is the mixture flow velocity. With

$$w_m = w_a + w_f \qquad \text{and} \qquad \theta = w_a/w_f$$

$$V_m = \frac{w_a(1 + 1/\theta)}{\rho_m A} \tag{5}$$

The density of the mixture, ρ_m, must be determined from a calculation of the volume percentage of fuel involved. A plot of mixture flow velocity versus air–fuel ratio for constant air-flow rates is shown in Fig. 3. The time required for the mixture to fill the tube completely is given by

$$t_m = L_0/V_m \tag{6}$$

where L_0 is the length of the tube in feet.

INJECTION VELOCITY

The injection velocity of the unburned mixture into the detonation tube may be calculated assuming incompressible flow.

$$(wV_i)_m = (wV_i)_a + (wV_i)_f$$

where w is the weight flow of fluid, V_i is the injection velocity, and the subscripts m, a, and f refer to mixture, air, and fuel, respectively. Using

$$w_m = w_a + w_f \qquad \text{and} \qquad w = \rho A_i V_i$$

where ρ is the density and A_i is the injection flow area, the mixture injection velocity is

$$V_{mi} = \frac{(w^2/\rho A_i)_a + (w^2/\rho A_i)_f}{w_a + w_f} \tag{7}$$

The assumption that Chapman-Jouguet detonation is established immediately at the closed end of the tube may only be approximated in the actual case. The detonation wave will be formed almost immediately after spark energization if the burning initiated by the spark is turbulent rather than laminar. Turbulent burning is induced by a reverse-flow fuel injector that directs the fuel flow diagonally rearward against the air flow. The vector relationships are

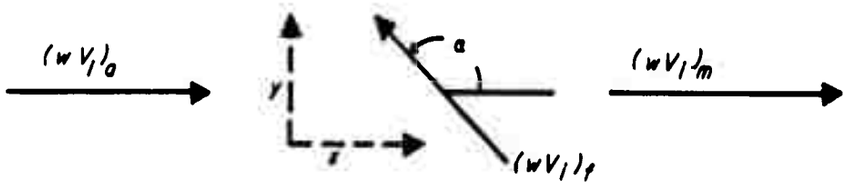

Since the momentum of the mixture, which is in the x direction, is not affected by the y-momentum component of the fuel momentum

$$(wV_i)_m = (wV_i)_a + (wV_i)_f \cos \alpha$$

where α is the angle of fuel impingement, measured counterclockwise from the direction of unburned mixture flow. Equation 7 becomes

$$V_{mi} = \frac{(w^2/\rho A_i)_a + (w^2/\rho A_i)_f \cos \alpha}{w_a + w_f}$$

Substituting $\theta = w_a/w_f$ and setting the constants

$$C = \frac{1}{A_{ai}\rho_a} \qquad \text{and} \qquad B = \frac{\cos \alpha}{A_{fi}\rho_f}$$

$$V_{mi} = w_a \frac{B + C\theta^2}{\theta(1 + \theta)} \tag{8}$$

A plot of Eq. 8 is shown in Fig. 4. Assuming an injection temperature of 100°F, a specific heat ratio of 1.4, an air–fuel ratio of 15.6 (stoichiometric), and an air flow rate of 0.0500 lb/sec, we find that the maximum Mach number of injection is 0.317. The maximum permissible Mach number at which flow may still be considered incompressible is about 0.3 (Ref. 17), so that the original assumption of incompressible flow is reasonably valid.

FREQUENCY OF SPARK ENERGIZATION

The frequency of spark energization, assuming that a detonation wave will be formed with every spark discharge, is given by

$$f = 1/t_c \tag{9}$$

where

$$t_c = t_d + t_{ex} + t_m$$

The detonation-wave travel time may be expressed as

$$t_d = L_0/V_d = L_0/M_1 a_1$$

where V_d is the velocity of the detonation wave with respect to the tube, M_1 is the Mach number of detonation, and a_1 is the speed of sound in the unburned gas.

The time for the tube to exhaust to atmospheric pressure is not known in general terms; an approximation based on Ref. 15 is used.

$$t_{ex} = L_0/a_2$$

where a_2 is the speed of sound in the burned gas. The speed of sound in the burned gas is determined from the temperature of the burned gas, which is given by the relation

$$\frac{T_2}{T_1} = \frac{m_2}{m_1}\frac{\gamma_2}{\gamma_1}\frac{1}{M_1^2}\left(\frac{1 + \gamma_1 M_1^2}{1 + \gamma_2}\right)^2 \tag{10}$$

where m is the molecular weight. For this case the molecular-weight ratio will be considered unity.

The time required for the unburned mixture to fill the tube, t_m, is given by Eq. 6.

It is readily seen that the detonation travel time, t_d, and the exhaust time, t_{ex}, depend on the Mach number of detonation, M_1, which is dependent on the air–fuel ratio, θ. The loading time, t_m, depends on both the air–fuel ratio and the air flow rate, with the air flow rate being the predominant factor. A plot of Eq. 9 is shown in Fig. 5. This is, of course, a highly idealized equation.

The frequency of operation of the intermittent-detonation device may be estimated with an error of less than 6% by neglecting the detonation and exhaust times in Eq. 9. An approximation of this type would be useful if detonation velocity data were not available for the proposed air–fuel combination.

THEORETICAL CALCULATIONS

Calculations were made for a propane–air mixture with the following physical characteristics for the detonation device:

$A_{ai} = 0.279$ in^2 $\qquad \alpha = 135$ degrees

$A_{fi} = 0.010$ in^2 $\qquad \gamma_1 = 1.4$

$\rho_a = 0.0765$ lb/ft^3 $\qquad \gamma_2 = 1.15$

$\rho_f = 0.1114$ lb/ft^3 $\qquad m_1 = m_2$

Calculated values for the constants B and C in Eq. 8 are

$$B = -100{,}654 \qquad \text{and} \qquad C = 6{,}743$$

The Mach number of detonation, M_1, for propane–air mixtures was taken from calculations made by Eisen, Gross, and Rivlin (Ref. 18) on an automatic digital computer. A plot of Mach number of detonation versus air–fuel ratio[1] is shown in Fig. 6.

EXPERIMENTAL EQUIPMENT

The experimental apparatus permitted the operating parameters—the air and fuel flow rates and the frequency of spark energization—to be independently varied (Fig. 7). Thrust was measured by a reaction balance. Air and fuel flow rates were measured with Fischer and Porter variable-area flowrators. Spark-energization frequency was recorded on a Honeywell Model 906 A Visicorder Oscillograph.

INTERMITTENT-DETONATION DEVICE

The intermittent-detonation device consists of three assemblies: the air manifold, the fuel injector, and the detonation tube. The air manifold (Fig. 8) consists of an inner and outer shell, both turned from mild steel. The outer manifold is fed by two air lines while the inner manifold has eight inlet ports whereby air is introduced into the detonation tube coaxially. The double-shell manifold design evolved from the single-shell design of a preliminary test device.

The fuel injector (Fig. 9) has three parts: a pintle, a sealing nut, and a reverse-flow diffuser. All parts were machined from brass. The pintle is a hollow tube that passes through the outer air-manifold shell and screws into the inner air-manifold headplate. The sealing nut screws into the outer air-manifold headplate and contains an O-ring that seats on the pintle to prevent air from passing back along the tube. The flat-face reverse-flow diffuser screws into the inner end of the pintle and directs the fuel flow rearward against the air flow at an angle of 45 degrees. The fuel injector used on the preliminary test device was a short length of 1/8-inch pipe. The fuel was injected coaxially with the air stream and mixing of the two streams was found to depend on the air–fuel ratio. The flat-face reverse-flow injector was substituted to retain the closed-end tube effect of the classical detonation apparatus while introducing the required mixture turbulence, since both are necessary for rapid transition from deflagration to detonation. In the air manifold and fuel injector assembly, shown in Fig. 10, the flat face of the reverse-flow injector almost closes the end of the detonation tube to provide the closed-end tube effect.

The detonation tube is made from 1 1/4-inch OD by 1-inch ID seamless steel tubing, 6 feet in length. One end is threaded externally to permit attachment to the air manifold. The ignition electrodes are provided by a standard 18-mm aircraft spark plug that screws into a threaded riser welded to the tube wall approximately 15 tube diameters downstream from the mixing plane.

[1] The extrapolation is based on a personal communication with Dr. R. A. Gross.

SPARK ENERGY SOURCE

A thyratron pulsing circuit was built that controlled the spark frequency satisfactorily; however, the spark was of insufficient energy to ignite the moving propane–air mixture. An automobile distributor was tried as a means of pulsing the induction coil primary. A standard 6-volt automobile coil provided ignition that resulted in spasmodic tube operation, and a more powerful induction coil of the scientific instrument type with spring-loaded breaker points did not lend itself to imposed frequency operation.

Use of an oil-filled Delco-Remy automobile induction coil resulted in satisfactory tube operation. The high-tension induction-coil primary is connected through a modified automobile distributor to a 12-volt d.c. power supply. The distributor is modified by increasing the capacitance across the breaker points from 0.18 to 8 millifarad to prevent point arcing caused by the high current drain of the coil. The distributor is direct-driven by a 1/5-horsepower, 27-volt d.c. motor–gear-train combination. The motor speed is controlled by varying the voltage with a 150-watt rheostat. The spark frequency can be varied from 1 to 60 cps. The distributor assembly is shown in Fig. 11.

THRUST MEASUREMENT

It was intended originally to measure the thrust output of the intermittent-detonation device by mounting the device in a specially designed test stand. The device was mounted on a plate that was attached to a firm base by two thin flexure plates. An electromechanical transducer was mounted so that one side of the transducer was connected to the movable upper plate while the outer side was attached to the firm base. Although this test stand proved quite sensitive, it had undesirable resonant-vibration characteristics and could not be used.

The device was then suspended as a pendulum with the manifold end connected directly to an electromechanical transducer. This thrust measuring apparatus also had undesirable resonant-vibration characteristics and was abandoned. The high-intensity spark caused the galvanometer in the oscillograph to jump, and no satisfactory solution to this problem was found.

A reaction balance (Fig. 12) was built that consisted of a movable mount restrained by an expansion spring. A device of this type had been used by Hoffman (Ref. 14). The mount consists of a cart on 4 ball-bearing rollers that move on the rails of an inverted 8-inch steel channel-section, 4 feet in length. The tops of the tails were milled and surface ground to provide a smooth surface. An 18-coil expansion spring, fabricated from 0.053-inch-diameter music wire, and the air hose leading to the cart provided the restraint for the system. After calibration with a dead-weight system, the thrust of the intermittent-detonation device was measured by noting the deflection of the cart along the channel on a scale attached to the inverted channel-section. This thrust-measuring system proved entirely satisfactory. Since it was completely mechanical, the high-intensity spark discharge had no effect. The one drawback to the system was that it measured only the average thrust; variation of thrust within each cycle could not be obtained. With the detonation tube in operation the cart was absolutely steady at frequencies above 15 cps. At frequencies below 15 cps a slight reciprocating motion was noted, and average readings were taken. Reproducibility was very good.

FLOW MEASUREMENT

Air was discharged from a Leroi compressor into a 200-cubic-foot storage tank, filtered by a replaceable cartridge filter, and passed through a Grove dome regulator that provided a constant-pressure flow output. The air temperature was measured by a dial thermometer, and the air flow by a factory-calibrated flowrator. The manufacturer states an accuracy of 1% of maximum flow for a calibrated meter. Upstream and downstream air pressures were read on Bourdon-tube pressure

gages. Air flow was controlled by a 3/4-inch globe valve placed on the downstream side of the flowrator. The air line between the control valve and the detonation-device manifold was 1-inch flexible air hose.

Propane was supplied from a 25-gallon (100 pounds) commercial propane cylinder placed in a hot water bath with the water temperature regulated to maintain a propane bottle pressure of at least 100 psi (Fig. 13). Propane was passed through a Grove dome regulator which provided a constant-pressure-flow output independent of flow rate. The temperature of the propane was measured by a dial thermometer and the flow by a flowrator. Upstream and downstream pressures were read on Bourdon-tube pressure gages. Propane flow was controlled by a 3/8-inch needle valve placed on the downstream side of the flowrator. The propane flow was carried to the detonation-device injector through a 1/4-inch high-pressure hose.

Dome pressure for the Grove regulators was supplied from a high-pressure nitrogen bottle.

Air and propane flow measurement and control apparatus along with other control instrumentation was grouped on a control panel, shown in Fig. 14.

EXPERIMENTAL PROCEDURE

GENERAL OBSERVATIONS

Preliminary runs at the University of Nebraska in February, 1959 showed that the detonation device was sensitive to certain physical parameters. The distance between the fuel-injection plane and the spark source determined whether the tube could be operated smoothly at various air flow rates. With the spark source near the injection plane the tube performed satisfactorily for low air flow rates. As the spark source was moved farther away from the injection plane the tube could be operated at high air flow rates, but did not work well at the lower air-flow rates.

The distance the spark electrodes projected into the detonation tube had a very decided effect on tube operation—a difference of a few hundredths of an inch determined whether the tube operated smoothly or spasmodically.

It was noted also that the detonation tube did not fire the same number of times per second that the ignition-coil primary was energized. It was shown that the spark plug was firing each time the coil primary was energized; therefore, it was concluded that the relationship between spark-electrode discharge and detonation-wave formation was a function of the wave interaction occurring within the tube. Since instrumentation for determining the formation of the detonation wave in the tube was not immediately available, it was decided to plot the data as a function of energization frequency and not of the actual firing rate of the detonation tube.

The above were general observations; no measurements were made to determine the exact effect of varying the parameters of the detonation device. The spark source was located 15 inches downstream from the fuel-injection plane. The projection of the spark electrodes into the tube was determined by operating the detonation device with the spark electrodes in various positions. The spark electrodes were fixed in that position which seemed to give smooth tube operation over the range of air–fuel ratios studied.

A plot of the power input to the ignition coil is shown in Fig. 15, along with the power output per spark discharge computed on the basis of a coil efficiency of 100%. The power input to the ignition coil primary was obtained by placing a Weston electrodynamometer wattmeter in the primary circuit. As the frequency of spark-coil energization increases, the power input to the coil primary decreases because of the shortened time interval the current has to build up against the inductive resistance of the primary winding. Lewis and Von Elbe (Ref. 19) indicate that the minimum ignition energy for stoichiometric propane–air mixtures at atmospheric pressure is about 0.26

millijoule. Figure 15 shows a power output of 0.65 joule at a spark-energization frequency of 60 cps. Thus, any difficulty in firing the propane–air mixture is the result of the physical placement of the spark electrodes with respect to the tube, and not the result of insufficient spark ignition energy.

An attempt was made to photogtaph the exhaust of the detonation tube with a 16-millimeter motion-picture camera using Eastman Tri-X film at a speed of 1,000 frames per second. The test was conducted at night so that the exhaust flame would be visible. The light from the flame was of sufficient intensity to record an image on the film on only one frame for each tube firing, and resolution of this frame was poor because of the high frame speed.

A test was made with an aluminum alloy detonation tube with a 1-inch OD and a length of 54 inches. The spark electrodes were located 15 inches from the fuel-injection plane. At an air flow rate of 0.0500 lb/sec and a frequency of spark energization at, or near, the upper resonant point, which is discussed under the heading Test Results, the aluminum alloy detonation tube failed structurally at a point about 8 inches from the exhaust end. It is believed that at or near this location the detonation wave is formed (see Appendix A). This failure occurred after about 2 minutes of operation at this frequency. Subsequent tests with the seamless steel detonation tube used in this investigation resulted in the steel tube bending from its own weight at the same approximate point at which failure occurred in the aluminum alloy tube. The steel tube was 72 inches in length. It should be noted that the calculated theoretical temperature immediately behind the detonation wave is in the order of 6300°R (Table 2). Heat transfer to the detonation-tube walls is increased because of the cyclic operation of the device. In the specific instances mentioned above, it was sufficient to cause complete or partial failure of the detonation tube.

TEST PROCEDURE

A test was started by adjusting the air flow rate to the desired value, adjusting the spark frequency by limiting the voltage input to the distributor drive motor with a rheostat, and admitting propane into the detonation tube. When the desired flow and frequency conditions had become stabilized, a record of flowrator readings, temperatures, and pressures was taken. The reaction-balance deflection was noted and a short length of oscillograph paper run off to record the spark-energization frequency. The thrust was measured for two series of tests: the air flow rate and spark frequency were fixed and the propane flow rate was varied to give different air–fuel ratios; and the air flow rate and air–fuel ratios were fixed and the spark frequency was varied.

Static calibration of the thrust measuring apparatus was made before and after each run. The calibration for a particular air flow rate was made with the air flow passing through the detonation tube. Therefore, all thrust values determined were net thrusts. An electric fan was always used to cool the ignition coil and also during the calibration. No difficulty was experienced in repeating calibration points.

TEST RESULTS

After the physical parameters of the detonation device were fixed, the effects of air–fuel ratio, air flow rate, and spark-energization frequency on tube operation were determined. The thrust produced by the discharge of the burned gas from the detonation tube yields the most information about tube operation. The thrust is a function of the pressure increase across the detonation wave and the frequency at which the tube fires. Therefore, data were taken for plots of thrust versus air–fuel ratio for various air flow rates and frequencies and for plots of thrust versus frequency for various air flow rates and air–fuel ratios. Plots of fuel specific impulse versus air flow rates indicated the amount of thrust produced per pound of fuel burned. Figures 16–27 are

plots of the test results. A line representing stoichiometric propane–air mixture has been drawn on each plot.

EFFECT OF AIR–FUEL RATIO ON THRUST

Figures 16–18 indicate the effect of air–fuel ratio on the thrust produced by the detonation tube for constant air flow rate and constant frequency of spark energization.

Figure 16 indicates the thrust variation for an air flow rate of 0.0400 lb/sec. The thrust increases with frequency until about 40 cps is reached; above 40 cps the thrust is reduced. The peak thrust occurs for all frequencies investigated at fuel-rich, air–fuel ratio of about 12.5.

Figure 17 is a plot of thrust versus air–fuel ratio for an air flow rate of 0.0500 lb/sec. The thrust increases with frequency until about 55 cps is reached; at 60 cps the thrust is reduced. Runs made at 8.5, 12, 20, 25, and 60 cps exhibit similar behavior with respect to thrust variation with air–fuel ratio. Runs at 33.5 and 40 cps exhibit a different behavior pattern from these, while the maximum-thrust run at 55 cps exhibits a third behavior pattern. The peak thrust occurs at an air–fuel ratio of about 12.5 for the runs made at 25, 33.5, 40, and 60 cps; at an air–fuel ratio of about 14 for the low frequency run, 8.5 cps; and at about 11.5 for the runs made at 12 and 20 cps. The maximum-thrust peak occurs at an air–fuel ratio of about 13.5 at 55 cps. All thrust peaks occur with fuel-rich mixtures.

Figure 18 shows the variation of thrust for an air flow rate of 0.0576 lb/sec. This was the maximum air flow rate investigated because of the flow capacity of the air flowrator. The thrust increases with frequency until about 55 cps is reached; at 59 cps the thrust has dropped considerably. Runs at 21 and 27 cps show that the peak thrust occurs at an air–fuel ratio of about 12; the low frequency run at 10 cps exhibits a constant thrust for a large range of air–fuel ratios. The 35- and 45-cps runs exhibit a marked reduction of thrust at an air–fuel ratio of about 11.5. The 55- and 59-cps runs exhibit similar behavior with the reduction of thrust being more pronounced in the 55-cps run. The maximum-thrust run at 55 cps exhibits a peak at an air–fuel ratio of about 13 and the run at 59 cps shows a peak at about 14.8. All thrust peaks occur with fuel-rich mixtures.

Morrison (Ref. 13), includes spark-schlieren photographs in his report which show that "clean" detonation fronts occur for hydrocarbon–oxygen mixtures which are slightly fuel rich. As the mixture becomes fuel lean the detonation front becomes an "interacting, nonhomogeneous region of shocks and combustion."

A review of the thrust variation with air–fuel ratio for constant air flow rate and constant frequency indicates the following:

1. The thrust increases to a maximum and then decreases as the frequency is increased for all air flow rates investigated.

2. The thrust increases with increasing air flow rate.

3. All thrust peaks occur with fuel-rich mixtures and with air–fuel ratios between 11 and 14 with the exception of the 10- and 59-cps runs at an air flow rate of 0.0576 lb/sec where the peak occurred at an air–fuel ratio of about 15.

4. Below 30 cps, the thrust increase to, and decrease from, the maximum is gradual. Between 30 cps and the maximum-thrust frequency the increase is more abrupt as the mixture becomes increasingly fuel rich, and the decrease is very abrupt especially for the 0.0500- and 0.0576-lb/sec air flow rates. For frequencies above the maximum-thrust frequency the thrust increases as the mixture becomes increasingly fuel rich and then, after the peak has been reached, decreases very gradually.

5. The maximum net thrust measured in the investigation was about 2.26 pounds; this occurred at an air flow rate of 0.0576 lb/sec, an air–fuel ratio of about 13, and a frequency of about 55 cps.

EFFECT OF SPARK-ENERGIZATION FREQUENCY ON THRUST

Figures 19–21 indicate the effect of spark-energization frequency on the thrust produced by the detonation device for constant air flow rates and constant air–fuel ratios.

Figure 19 shows that the thrust apparently reaches a peak at two frequencies at an air flow rate of 0.0400 lb/sec. For all air–fuel ratios plotted, the thrust increases with frequency until, at about 45 cps, the thrust remains essentially unchanged as the frequency is increased. The rate at which the thrust increases appears to decrease at about 25 cps and then reaches a well defined maximum at about 40 cps, with the exception of the very fuel-rich mixture of 9.79, which reaches a peak at about 45 cps. The maximum-thrust peak occurs for an air–fuel ratio of about 12.6 and a frequency of about 40 cps. The improved performance of the detonation device at the upper resonant frequency was very noticeable from the acoustic output of the tube. As the spark frequency was increased slightly, the frequency of tube operation increased very noticeably.

Figure 20 is a plot of thrust versus spark frequency for an air flow rate of 0.0500 lb/sec. The double thrust peak is again prominent for this air flow rate. The first peak appears to occur at about 25 cps and the second, larger, peak occurs at about 48 cps (the acoustic output indicated the general shape of the curve as shown) for an air–fuel ratio of about 17 (slightly fuel lean) with the peak for the other air–fuel ratios occurring at about 55 cps. The peak for the maximum-thrust run occurred for a fuel-rich air–fuel ratio of about 12.95.

Figure 21 is a plot of thrust versus spark frequency for an air flow rate of 0.0576 lb/sec. Again the thrust peaks are the predominant factor. The peak at the lower frequency is considerably damped when compared with the peak at the lower frequency for the air flow rates previously examined; the peak at the upper frequency is very distinct for all air–fuel ratios plotted. The abrupt decrease in thrust was very noticeable from the acoustic output of the tube. Firing became spasmodic for frequencies above 55 cps.

A review of the thrust variation with the frequency of spark energization for constant air flow rates and constant air–fuel ratios indicates the following:

1. The thrust increases with the frequency, reaching a maximum value at frequencies between 39 and 55, depending on air flow rate.

2. Two thrust peaks appear on the thrust versus frequency plots. The first, at a frequency of about 25 cps, is not as dominant as the upper peak, which occurs at frequencies between 39 and 55 cps.

3. As the air flow rate increases the upper thrust peak occurs at higher frequencies while the lower peak appears to remain at about 25 cps.

EFFECT OF AIR–FUEL RATIO ON FUEL SPECIFIC IMPULSE

Figures 22–24 indicate the effect of air–fuel ratio on the fuel specific impulse for constant air flow rate and constant frequency.

Figure 22 is a plot of fuel specific impulse versus air–fuel ratio for an air flow rate of 0.0400 lb/sec. Examination shows that the specific impulse increases with spark frequency, reaching a maximum at about 40 cps and then decreasing as the frequency is increased. The curves appear to reach maxima at air–fuel ratios between 14.5 and 16 for all frequencies except the 60-cps run, which reaches a maximum at an air–fuel ratio of about 13.

Figures 16 and 22 show that the specific impulse, when compared with the thrust, reaches a maximum at air–fuel ratios at, or near, the stoichiometric ratio. Although the thrust produced at near-stoichiometric air–fuel ratios is less than that produced for fuel-rich mixtures, the amount of fuel consumed is also less. The effect of burning less fuel is more dominant than the smaller thrust output, resulting in a greater specific impulse.

Figure 23 is a plot of fuel specific impulse versus air–fuel ratio for an air flow rate of 0.0500 lb/sec. The same results appear as were described for Fig. 22 with the exception of the maximum specific impulse occurring at about 55 cps and the maximum specific impulse for the 60-cps run occurring at about stoichiometric rather than at a fuel-rich condition.

Figure 24 is a plot of fuel specific impulse versus air–fuel ratio for an air flow rate of 0.0576 lb/sec. Again, the specific impulse increases with frequency to a maximum and then decreases as the frequency is increased. The maximum specific impulse for each constant frequency run appears to occur at, or near, the stoichiometric ratio. As exhibited also by Fig. 23, the specific impulse appears to decrease rapidly for air–fuel ratios more fuel rich than about 12 for frequencies between 30 and 50 cps. For other air–fuel ratios the decrease is not so abrupt.

A review of the fuel specific impulse variation with air–fuel ratio for constant air flow rate and constant frequency indicates the following.

1. The specific impulse increases with frequency, reaching a maximum and then decreasing with an increase in frequency.

2. The specific impulse increases with air flow rate.

3. For runs at constant frequency, the specific impulse attains a maximum value at or near the stoichiometric air–fuel ratio.

4. The maximum specific impulse computed for the investigation was about 560 lb-sec/lb, which occurred for an air flow rate of 0.0576 lb/sec, an air–fuel ratio of about 14.7, and a frequency of 55 cps.

EFFECT OF SPARK-ENERGIZATION FREQUENCY ON FUEL SPECIFIC IMPULSE

Figures 25–27 indicate the effect of spark-energization frequency on the fuel specific impulse for constant air flow rates and constant frequencies. Results are similar to the results of thrust versus spark frequency shown in Fig. 19–21 except that the maximum specific impulse values occur at, or near, the stoichiometric air–fuel ratio and the maximum thrust values occur at fuel-rich air–fuel ratios.

EXPERIMENTAL AND THEORETICAL CORRELATION

A comparison of the theoretical and maximum experimental thrust is shown in Fig. 28. The theoretical thrust equation, Eq. 3, is

$$F_{av} = \frac{t_{ex}}{t_c} A P_1 \left[\left(\frac{1 + \gamma_1 M_1^2}{1 + \gamma_2} \right) \left(1 - \frac{\gamma_2 - 1}{2} M_{2c} \right)^{2\gamma_2/(\gamma_2 - 1)} - 1 \right]$$

Values are calculated for air flow rates of 0.0400, 0.0500, and 0.0600 lb/sec. Aside from the obvious difference in thrust levels, the theoretical plots show little thrust variation with air–fuel ratio whereas the experimental curves show a definite dependency on air–fuel ratio.

Equation 3 was plotted with the cycle time, t_c, determined by Eq. 9, which is plotted in Fig. 5. The cycle time, t_c, is composed of three elements, two of which may be considerably in error. The time for the detonation wave to travel to the end of the tube, t_d, is very small, being

of the order of 0.00094 second. The Mach number of detonation, M_1, from which t_d is calculated, must be considered as being a satisfactory value for this parameter. The values obtained by the computer program, Ref. 18, agree with experimental data available in the literature. Therefore, the detonation wave travel time, t_d, will be considered satisfactory for the purpose of determining the cycle time.

As stated previously, the exhaust time, t_{ex}, is not readily determinable in an analytical form, being entirely dependent on the wave interaction phenomena occurring within the detonation tube. For the purpose of plotting Eq. 3, the exhaust time was defined as the time required for a single rarefaction wave, traveling at the sound velocity of the burnt gas, to move from the open to the closed end of the detonation tube. This probably yields an exhaust time less than the actual value. As shown in the wave diagram, Fig. 1, and discussed in the explanation of the wave diagram, a centered expansion fan occurs within the tube when the detonation wave reaches the end of the tube. Atmospheric pressure within the tube is not achieved until some later time. Therefore, the assumption of a single wave accomplishing the same results as a fan of waves should result in an exhaust time less than the actual value. Since, in Eq. 3, the exhaust time appears in both the numerator and denominator, the effect of choosing an incorrect exhaust time is reduced. The effect of choosing an exhaust time less than the actual value is to decrease the magnitude of the theoretical thrust. Yet, it is seen from Fig. 28 that the theoretical thrust values are greater than the actual thrust values for each air flow rate investigated.

The time required for the tube to fill with unburned mixture, t_m, appears in the denominator of Eq. 3 and is by far the largest of the three elements composing the cycle time. The unburned-mixture flow velocity, based on continuity considerations, is given by Eq. 5, and is plotted in Fig. 3. From this plot the average order of magnitude of the loading time is about 0.045 second. This value is about 25 times the exhaust time and about 50 times the detonation wave travel time. The effect of choosing a loading time that is long when compared with the actual value is to decrease the magnitude of the theoretical thrust. It is therefore concluded that the actual loading time for the intermittent-detonation tube is longer than that calculated for plotting of Eq. 3. Figure 5 is a plot of the theoretical operating frequency of the detonation tube based on the assumptions discussed above for the elements of the cycle time. One must conclude that the actual operating frequencies of the detonation tube are lower than those shown in Fig. 5. It is noted that these operating frequencies are lower than the spark-energization frequencies shown in Fig. 28. It was observed in the experimental runs that the actual operating frequency was always much lower than the spark-energization frequency. This was determined from the audio output of the tube and no comparative values were recorded.

A further observation may be made with regard to Fig. 28. The theoretical equations assume that optimum wave interaction occurs for all operating conditions under which the tube may be run. The experimental results, however, indicate that a particular combination of air flow rate, spark-energization frequency, and air–fuel ratio results in optimum or peak performance. Thus the theoretical analysis indicates little change with varying operating parameters, while the experimental results show a decided dependency on particular operating conditions. In this respect it is interesting to note that the difference between the theoretical thrust and the maximum experimental thrust, for each air flow rate shown in Fig. 28, is about 0.80 pound.

Another factor that must be considered, when comparing the theory with the experimental results, is the boundary conditions imposed on the exhaust of the burned gas from the detonation tube. In the present investigation, the discharge from the detonation tube was from a constant-area tube, thus limiting the exhaust velocity to that of the sound velocity in the burned gas. A properly shaped expansion section attached to the end of the tube would allow the exhaust gas to become supersonic, thereby increasing the thrust produced by the tube. The wave diagram, Fig. 1, shows that a centered expansion fan reduces the pressure within the tube. However, this fan extends

outside the tube also and reduces the exhaust gas pressure to that of the atmosphere. For a constant-area tube this expansion occurs outside the tube. If the reduction to atmospheric pressure at the open end of the tube can occur in an expansion section, the result will be an increase in the thrust produced by the tube. For pressure ratios encountered in the detonation tube this expansion will result in supersonic flow in the expansion section.

A comparison of the theoretical and experimental specific impulse is shown in Fig. 29. The theoretical specific impulse equation, Eq. 4, is

$$I_{sp} = \frac{t_{ex}}{t_c} \frac{A P_1 \theta}{w_a} \left[\left(\frac{1 + \gamma_1 M_1^2}{1 + \gamma_2} \right) \left(1 - \frac{\gamma_2 - 1}{2} M_{2c} \right)^{2\gamma_2/(\gamma_2 - 1)} - 1 \right]$$

Since the fuel specific impulse is given by

$$I_{sp} = \frac{F_{av}}{w_f}$$

the arguments that were applied to Eq. 3 may also be applied to Eq. 4. The amount of fuel, w_f, used to determine the fuel specific impulse is the same for both the theoretical and experimental calculations. It is noted, however, that the slopes of the theoretical and experimental data plots, Fig. 29, are approximately the same for air–fuel ratios between 10 and 15. Some variation with air–fuel ratio does occur, however, for the experimental specific impulse.

A comparison of the results of this investigation and those of Hoffman (Ref. 14) and Nicholls (Ref. 15) indicate similarities in many respects. Both of the previous investigators reported the effect of the distance between the fuel-injection plane and the spark source on detonation-tube operation. Nicholls reported that the thrust increased with frequency to a maximum and then decreased with increasing frequency; that the thrust increased with air flow rate; and that best tube operation occurred with fuel-rich mixtures. A comparison of Fig. 29 with a similar plot of their results for hydrogen–air mixtures indicates that the slopes of the theoretical and experimental specific impulse plots are approximately the same. In both cases the specific impulse increases as the mixture becomes fuel lean; however, in contrast with the results of this investigation, they obtained greater specific impulse values for lower air flow rates.

Hoffman reported that detonation-tube firing occurred at a frequency lower than the spark-energization frequency. Nicholls did not apparently find this to be true.

The maximum specific impulse and maximum thrust as functions of air–fuel ratio and air flow rate are shown in Fig. 30. The maximum specific impulse occurs at slightly fuel-lean mixtures for the lower air flow rates and at slightly fuel-rich mixtures for the higher air flow rates. In contrast, the maximum thrust occurs at fuel-rich mixtures for all air flow rates investigated. As the air flow rate is increased the maximum thrust occurs at slightly less fuel-rich mixtures. It should be noted that the maximum specific impulse and maximum thrust for each air flow rate occur at the same spark frequency.

The limits, in terms of air–propane ratio, at which the detonation device would fire were determined (Fig. 31). Each point plotted represents a number of different frequencies. For each air–fuel ratio, the limits of detonability for all frequencies investigated were about the same.

CONCLUSIONS

The following conclusions were drawn from the theoretical and experimental investigations of an intermittent-detonation device with physical parameters described herein operating with propane–air mixtures at air flow rates between 0.0400 and 0.0576 lb/sec.

1. A method of characteristics solution of the wave-interaction phenomena occurring during the discharge of burned gas from the detonation tube, if based on isentropic-flow conditions, does not yield results that are meaningful for exact physical quantities, but shows the general trend of the wave phenomena occurring within the tube.

2. A theoretical determination of the operating frequency of the detonation device, based on idealized assumptions, results in frequencies that are high when compared with experimental results.

3. Expressions for the thrust and fuel specific impulse, based on the assumptions of Ref. 15, give results that are greater than the experimental results.

4. The position of the spark source with respect to the fuel-injection plane is important for satisfactory tube operation and determines the air flow rates at which the tube may be operated satisfactorily.

5. The distance that the spark electrodes project into the detonation tube has a decided effect on the smooth operation of the detonation device.

6. The thrust and fuel specific impulse of the detonation device increase with frequency to a maximum and then decrease as the frequency is increased.

7. The thrust and fuel specific impulse increase with air flow rate.

8. The frequency of spark energization at which maximum thrust and fuel specific impulse occur increases as the air flow rate is increased.

9. Two thrust peaks appear on the thrust versus frequency plots. The lower frequency peak is not as abrupt or dominant as the higher frequency peak. The device appears capable of operating at one or more resonant frequencies.

10. Maximum thrust for constant frequency operation occurs for fuel-rich mixtures for all air flow rates investigated.

11. Maximum fuel specific impulse for constant frequency operation occurs at or very near to the stoichiometric air–fuel ratio.

12. The intermittent-detonation device, using gaseous detonative combustion, does not appear promising as a thrust producing mechanism for propulsion. An intermittent thrust producer requires rapid cyclic operation (of the order of 1,000 cps) to be competitive with steady-flow devices. The reloading of a long tube with gaseous mixture between cycles limits the gaseous intermittent-detonation device to low cycling rates.

RECOMMENDATIONS

The investigation of intermittent-detonative combustion should be continued to determine the conditions under which resonant operation occurs. The effects of varying the physical characteristics of the detonation device should be determined quantitatively.

An analytical and experimental investigation of the effects of exhaust diffusers of various geometrical shapes should be considered.

Appendix A
TRANSITION FROM DEFLAGRATION TO DETONATION

The mechanism whereby a deflagration wave (combustion wave) accelerates and undergoes a transition to a detonation wave in a closed tube with a multifold increase in velocity, pressure, and temperature has been the subject of experimental and theoretical activity for many years. Until recently, not even a qualitative explanation could be made of this transition process. In the last few years, however, progress has been made in this respect and a reasonably substantial explanation can now be given of this phenomenon.

For the device described herein, the following phenomenological description of the transition from deflagration to detonation may be given.

1. The combustible mixture is ignited by an electric spark at the closed end of the tube and a flame, proceeding from the closed end of the tube, sends out a preflame shock that heats and compresses the unburned gas. The original strength of this shock is dependent on the amount of electrical energy released in the spark discharge. The flame accelerates as it overruns the shock-treated mixture so that stronger compression waves are sent out. The continual overrunning of the flame into the shock-treated mixture is of importance only in the initial stages of the transition process.

2. If the combustible mixture were laminar at ignition, a laminar flame would result. Tube-wall friction would gradually cause the flow to become turbulent and this, in turn, would cause the laminar flame to become turbulent. The turbulent flame, because of its wrinkled and folded structure, sends out intermittent pressure pulses which cause the propagating flame to accelerate still further. Pressure pulses are sent out by the turbulent flame in two directions: toward the unburned mixture, and toward the closed end of the tube. The pressure pulse sent toward the closed end of the tube is reflected and reinforces the preflame shock, thereby increasing the flame propagation speed. The effect of reflected waves on the acceleration of the flame is much more appreciable than the acceleration caused by the overrunning of the shock-treated mixture.

The preflame shock is reinforced by the above mechanism until it becomes strong enough to cause the mixture between flame and shock to ignite spontaneously locally, further strengthening the shock so that successive ignitions occur spontaneously closer and closer to the shock. When autoignition occurs at the shock front, the shock is highly accelerated, and the detonation wave is formed.

3. In the case of the device described in this report the mixture is turbulent upon ignition so that a highly turbulent flame is established immediately. The acceleration of the flame is therefore very rapid because of the early production of intermittent pressure pulses by the turbulent flame.

Appendix B
METHOD OF CHARACTERISTICS—UNSTEADY FLOW

The fundamental, nonlinear, partial-differential equations that describe the flow of compressible fluids are too complicated to be solved directly. Generally, these equations are reduced to a manageable form by omitting terms that are of small magnitude for the problem under investigation. The method of characteristics is a graphical and numerical method of solving the partial-differential equations that describe the flow of a compressible fluid. For the problem treated in this report the flow is unsteady, i.e., the flow properties depend not only on distance but also on time.

For unsteady flow in a constant-area duct a flow problem is completely solved once the state of the gas and its flow velocity are known at all times and at all points in the duct. Particularly convenient parameters are the flow velocity relative to the duct, the local speed of sound, and the specific entropy. The procedure is greatly simplified by the use of dimensionless quantities involving the above stated parameters. A reference state, indicated by the subscript zero, is selected. The following dimensionless quantities are therefore defined:

$$\mathfrak{a} = \frac{a}{a_0}, \qquad U = \frac{u}{u_0}, \qquad S = \frac{s}{C_p(\gamma - 1)}$$

$$\mathfrak{a}_0 = 1, \qquad S_0 = s_0 = 0$$

where a is the local speed of sound, a_0 is the speed of sound in reference state, u is the flow velocity relative to the duct, s is the specific entropy, and s_0 is the specific entropy of the reference state. For the problem under consideration the entropy of all particles is the same and constant, since isentropic flow was assumed.

The independent variables of the problem are the distance and time coordinates, x and t, respectively. These are made dimensionless by selecting a reference length L_0. Thus

$$\xi = \frac{x}{L_0}, \qquad \tau = \frac{a_0 t}{L_0}$$

The detailed mathematical derivation of the characteristics relations is considered to be outside the scope of this appendix. The characteristics relations are obtained by writing the equations of continuity, momentum, and entropy, and including the equation of state of the fluid under consideration. After rearrangement and substitution, three types of characteristics curves are obtained, defined by the equation

$$\frac{d\xi}{d\tau} = U + \mathfrak{a}, \qquad \frac{d\xi}{d\tau} = U - \mathfrak{a}, \qquad \frac{d\xi}{d\tau} = U$$

Curves of the direction $U + \mathfrak{a}$ are referred to as P-waves, and curves of $U - \mathfrak{a}$ as Q-waves. The curves of direction U are the paths of fluid elements. The plot showing the propagation of characteristics in the ξ,τ-plane is called a wave diagram.

For isentropic flow the problem reduces to one with two dependent variables only. The values of P and Q remain constant along their respective characteristics. The magnitudes of P and Q are given by

$$P = \frac{2}{\gamma - 1} a + U \qquad \text{and} \qquad Q = \frac{2}{\gamma - 1} a - U$$

The assumption of isentropic flow permits the computation of P, Q, a, and U by numerical techniques, based on the known boundary conditions of the problem, rather than a graphical technique, which would be necessary if nonisentropic flow has been considered.

The effect of any disturbance of local flow conditions can be felt at other points only after the P- and Q-waves that pass through the origin of the disturbance arrive there. The characteristics are thus signals which carry information about local flow disturbances to other parts of the duct. If the flow is steady, i.e., does not depend on time, then the P- and Q-waves become two families of parallel curves. As a result of flow disturbances, the characteristics will no longer remain parallel but will either diverge or converge.

Wave diagram procedures are usually applied only within regions that are bounded either by the ends of the duct or by discontinuities. The ends of a duct can only be reached by either P-waves or Q-waves, depending on whether the right or the left end of the duct is considered. For the wave diagram shown in Fig. 1, the closed end of the duct is reached only by Q-waves and the open end of the duct only by P-waves.

The boundary condition at the closed end of the duct is given by the fact that the flow velocity there must be zero. When the fresh mixture charge begins to flow into the duct the boundary condition is given by the velocity of the interface, for points above point 39 in Fig. 1.

The boundary condition at the open end of the duct depends on whether the outflow is subsonic, sonic, or supersonic. For subsonic outflow, with the gas in the external region at rest, the pressures at the exit and in the external region are equal. For sonic exit velocities the exit pressure may be larger than the external pressure. This boundary condition is represented by

$$U_{exit} = a_{exit}$$

Since supersonic outflow is not present in the problem under consideration, it will not be discussed here.

The pressure ratio for a particular wave diagram point is given by

$$p/p_1 = (a/a_1)^{2\gamma/(\gamma-1)} e^{-\gamma(S-S_1)}$$

in terms of the dimensionless variables defined previously. For isentropic flow this reduces to

$$p/p_1 = (a/a_1)^{2\gamma/(\gamma-1)}$$

To illustrate the computational procedure, two examples from Fig. 1 and Table 1 will be given.

The computation of conditions at point 21 in Fig. 1 is as follows: point 21 lies on the P-wave which includes points 18–20. Since points on this wave, in isentropic flow, have the same characteristics values, point 21 has the same P value as points 18–20. This value, from Table 1, is 14.22. The value of Q at point 21 is the same as that of Q at points 6 and 14. This value is 13.41. From the relations for P and Q

$$P = \frac{2}{\gamma - 1} a + U$$

$$Q = \frac{2}{\gamma - 1} a - U$$

the values of U and a for point 21 are 0.405 and 1.035, respectively. With the slopes of the characteristics from point 21 known, it is now possible to proceed to point 22.

The computation of conditions at point 25, which is at the closed end of the tube, is as follows: The flow velocity at the closed end of the tube must be zero, except at the interface between the fresh mixture and burned gas where the velocity is given by the interface velocity. For point 25 the pressure at the closed end of the tube is greater than atmospheric, indicating that the fresh mixture has not yet begun to flow into the tube. Therefore, the flow velocity is zero. The value of Q at point 25 is 13.93, being the same as that at points 4, 12, and 19. Since U is zero, the value of P is equal to that of Q at point 25. With P, Q, and U known, the value of $\mathfrak{A}$ is easily determined. The pressure ratio at point 25 is given by

$$p/p_1 = (\mathfrak{A}/\mathfrak{A}_1)^{2\gamma/(\gamma-1)}$$

The magnitude of $\mathfrak{A}_1$ is one from the original conditions of the problem. The value of the ratio of specific heats is 1.15, also obtained from the original conditions. The pressure ratio value is, therefore,

$$p/p_1 = (\mathfrak{A})^{15.3} = (1.043)^{15.3} = 1.905$$

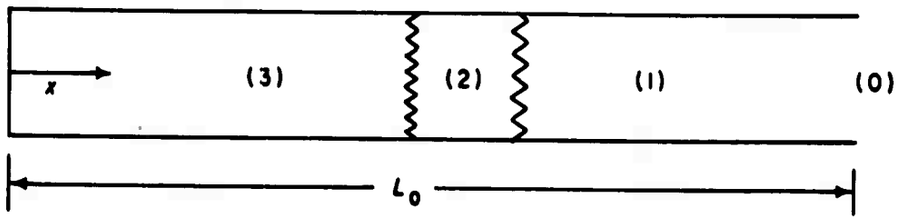

NOTE: The numbers in this figure indicate the subscript notation: 0, initial conditions; 1, conditions in unburned gas; 2, conditions in burned gas behind detonation wave; and 3, conditions in burned gas behind trailing rarefaction wave.

TABLE 1. DATA SHEET FOR METHOD OF CHARACTERISTICS, NONSTEADY FLOW

Assumed conditions are air flow rate, 0.0500 lb/sec; $\theta = 15.6$, stoichiometric; $M_1 = 5.6$ (Fig. 6); $p_0 = p_1 = 1$ atmosphere; $T_0 = T_1 = 560°R$; $a_0 = a_1 = 1{,}150$ ft/sec; and $\gamma_0 = \gamma_1 = 1.4$, $\gamma_2 = \gamma_3 = 1.15$. Calculated conditions are $p_3/p_1 = 8$ (Eq. 1), $L_0 = 6$ feet, $a_0/L_0 = 192$.

Point	P	Q	U	Ω	$U + \Omega$	$U - \Omega$	p/p_0	W
1	15.3	15.3	0	1.146	1.146	-1.146	8	.....
2	15.3	14.76	0.27	1.125	1.395	-0.855	.....	.....
3	15.3	14.22	0.54	1.105	1.645	-0.565	.....	.....
4	15.3	13.93	0.685	1.095	1.780	-0.410	.....	.....
5	15.3	13.68	0.81	1.085	1.895	-0.275	.....	.....
6	15.3	13.41	0.945	1.075	2.020	-0.130	.....	.....
7	15.3	13.24	1.03	1.07	2.10	-0.03	.....	.....
8	15.3	13.188	1.056	1.068	2.124	-0.012	.....	.....
9	15.3	13.135	1.065	1.065	2.13	0	2.62	.....
10	14.76	14.76	0	1.105	1.105	-1.105	4.62	.....
11	14.76	14.22	0.27	1.085	1.355	-0.815	.....	.....
12	14.76	13.93	0.415	1.075	1.490	-0.660	.....	.....
13	14.76	13.68	0.54	1.065	1.065	-0.525	.....	.....
14	14.76	13.41	0.675	1.054	1.729	-0.379	.....	.....
15	14.76	13.24	0.76	1.05	1.81	-0.29	.....	.....
16	14.76	13.188	0.786	1.045	1.831	-0.259	.....	.....
17	14.76	12.72	1.03	1.03	2.06	0	1.573	.....
18	14.22	14.22	0.147	1.065	1.065	-1.065	2.62	.....
19	14.22	13.93	0.27	1.052	1.199	-0.905	.....	.....
20	14.22	13.68	0.27	1.045	1.315	-0.775	.....	.....
21	14.22	13.41	0.405	1.035	1.44	-0.630	.....	.....
22	14.22	13.24	0.490	1.028	1.518	-0.538	.....	.....
23	14.22	13.188	0.516	1.026	1.542	-0.510	.....	.....
24	14.22	12.48	0.87	1.00	1.87	-0.13	1.00	.....
25	13.93	13.93	0	1.043	1.043	-1.043	1.905	.....
26	13.93	13.68	0.125	1.035	1.160	-0.910	.....	.....
27	13.93	13.41	0.26	1.023	1.283	-0.763	.....	.....
28	13.93	13.24	0.345	1.017	1.362	-0.672	.....	.....
29	13.93	13.188	0.371	1.015	1.386	-0.644	.....	.....
30	13.93	12.48	0.725	0.99	1.715	-0.265	.....	.....
31	13.93	12.77	0.580	1.00	1.58	-0.42	1.00	.....

TABLE 1. (CONTD.)

Point	P	Q	U	$\hat{q}$	$U+\hat{q}$	$U-\hat{q}$	p/p_0	W
32	13.68	13.68	0	1.022	1.022	-1.022	1.396	.....
33	13.68	13.41	0.135	1.015	1.150	-0.880	.....	.....
34	13.68	13.24	0.22	1.008	1.228	-0.788	.....	.....
35	13.68	13.188	0.246	1.005	1.251	-0.759	.....	.....
36	13.68	12.48	0.60	0.98	1.58	-0.38	.....	.....
37	13.68	12.77	0.455	0.99	1.445	-0.535	.....	.....
38	13.68	13.02	0.33	1.00	1.33	-0.67	1.00	.....
39	13.41	13.41	0	1.005	1.005	-1.005	1.079	.....
40	13.41	13.24	0.085	0.998	1.083	-0.913	.....	.....
41	13.41	13.188	0.111	0.996	1.107	-0.885	.....	.....
42	13.41	12.48	0.465	0.97	1.435	-0.505	.....	.....
43	13.41	12.77	0.32	0.98	1.30	-0.66	.....	.....
44	13.41	13.02	0.195	0.99	1.185	-0.795	.....	.....
45	13.41	13.29	0.06	1.00	1.06	-0.94	1.00	.....
46	13.463	13.24	0.113	1.00	1.113	-0.887	1.00	.....
47	13.463	13.188	0.1375	0.998	1.136	-0.861	.....	.....
48	13.437	12.48	0.4783	0.97	.....	.....	.....	.....
49	13.437	12.77	0.333	0.983	.....	.....	.....	-0.582
50	13.463	12.48	0.491	0.97	1.461	.....	.....	.....
51	13.463	12.78	0.341	0.995	1.336	-0.654	.....	-0.569
52	13.463	13.02	0.221	0.993	1.214	-0.772	.....	.....
53	13.463	13.29	0.087	1.00	1.087	-0.913	.....	.....
54	13.463	13.237	0.113	1.00	1.113	-0.887	1.00	.....
55	13.413	13.188	0.113	0.998	1.111	-0.885	.....	.....
56	13.413	12.48	0.467	0.97	1.437	-0.503	.....	.....
57	13.413	12.78	0.317	0.98	1.297	-0.663	.....	-0.538
58	13.413	13.02	0.197	0.99	1.187	-0.793	.....	.....
59	13.413	13.29	0.061	1.00	1.061	-0.939	.....	.....
60	13.413	13.237	0.088	0.999	1.087	-0.911	.....	.....
61	13.413	13.287	0.063	1.00	1.063	-0.937	1.00	.....

TABLE 2. COMPUTATIONS FOR EQ. 3 AND 4.

Quantity	θ						
	8	10	12	14	15.6	16	18
M_1	5.53	5.56	5.58	5.59	5.61	5.58	5.43
M_1^2	30.58	30.91	31.14	31.25	31.47	31.08	29.48
$\gamma_1 M_1^2$	42.81	43.27	43.60	43.75	44.06	43.51	41.27
$1/M_1^2$	0.0327	0.0324	0.0321	0.0320	0.0318	0.0322	0.0339
$\frac{1+\gamma_1 M_1^2}{1+\gamma_2} = \frac{p_2}{p_1}$	20.38	20.59	20.74	20.81	20.96	20.70	19.66
$\left(\frac{1+\gamma_1 M_1^2}{1-\gamma_2}\right)^2$	415.34	423.95	430.15	433.06	439.32	428.49	386.52
T_2/T_1	11.16	11.28	11.34	11.38	11.48	11.33	10.76
T_2	6250	6317	6350	6373	6429	6345	6026
a_2	3515	3530	3540	3545	3562	3540	3450
V_d	6360	6394	6417	6429	6452	6411	6245
V_d/a_2	1.809	1.811	1.813	1.813	1.811	1.811	1.810
M_{2c}	0.809	0.811	0.813	0.813	0.811	0.811	0.810
$1-\frac{\gamma_2-1}{2}M_{2c}$	0.939	0.939	0.939	0.939	0.939	0.939	0.939
$\left(1-\frac{\gamma_2-1}{2}M_{2c}\right)^{15.33}$	0.382	0.382	0.382	0.382	0.382	0.382	0.382
p_3/p_1	7.785	7.865	7.923	7.95	8.00	7.91	7.51
$1/a_2$	0.000284	0.000283	0.000282	0.000282	0.000281	0.000282	0.00029
$1/V_d$	0.000157	0.000156	0.000156	0.000156	0.000155	0.000156	0.000160

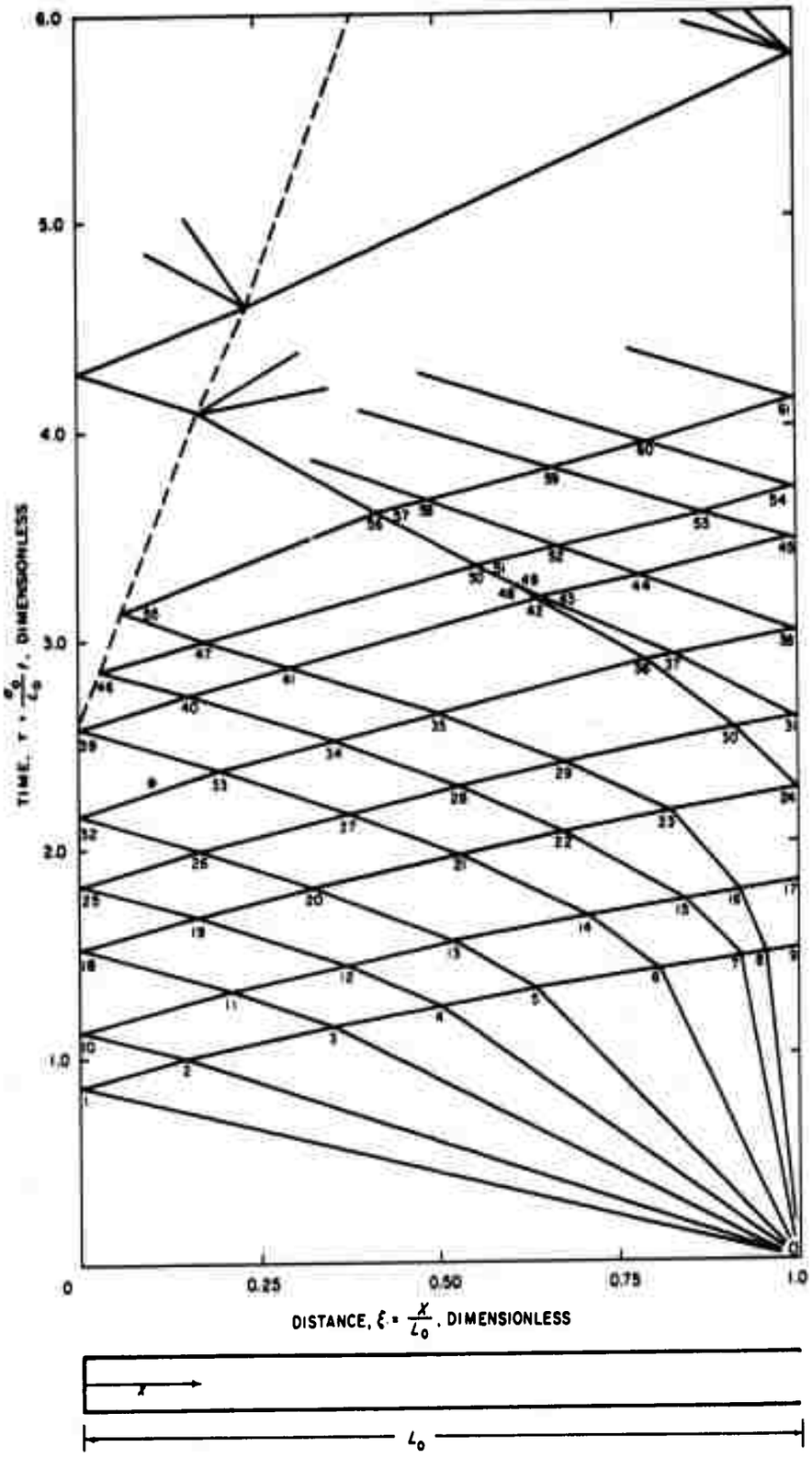

FIG. 1. Wave Diagram, Isentropic Discharge of Detonation Tube.

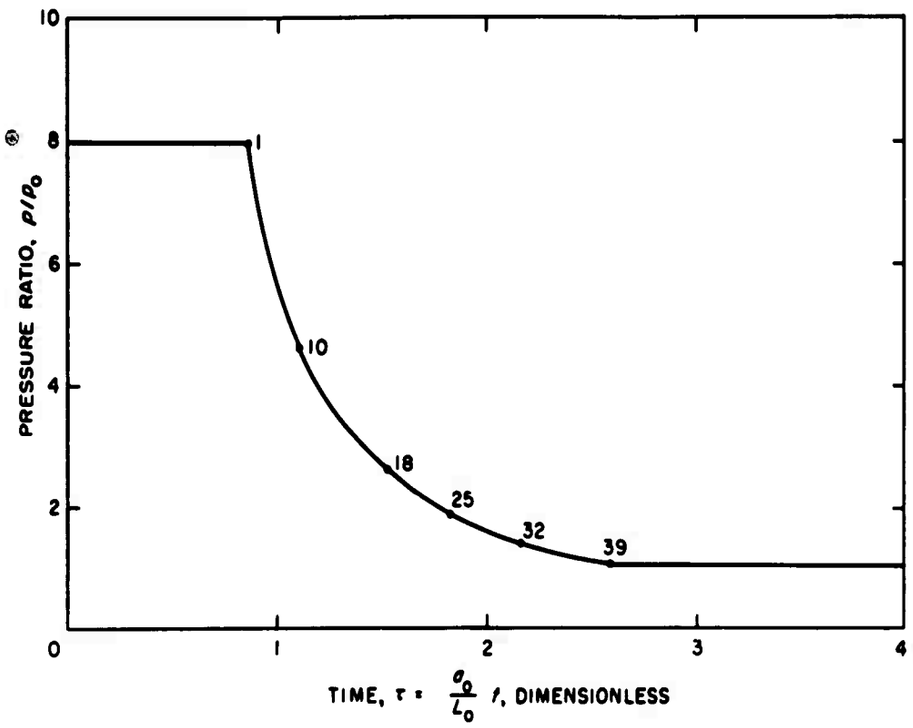

FIG. 2. Pressure Decay at Closed End of Duct as Determined by Method of Characteristics.

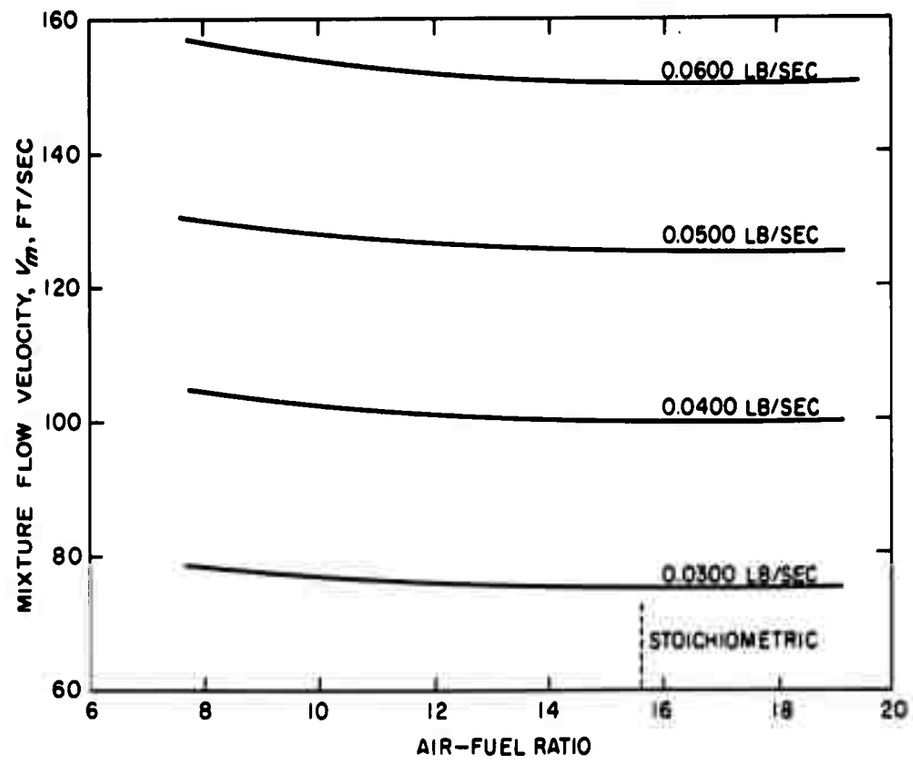

FIG. 3. Theoretical Mixture Flow Velocity Versus Air–Fuel Ratio for Various Air Flow Rates.

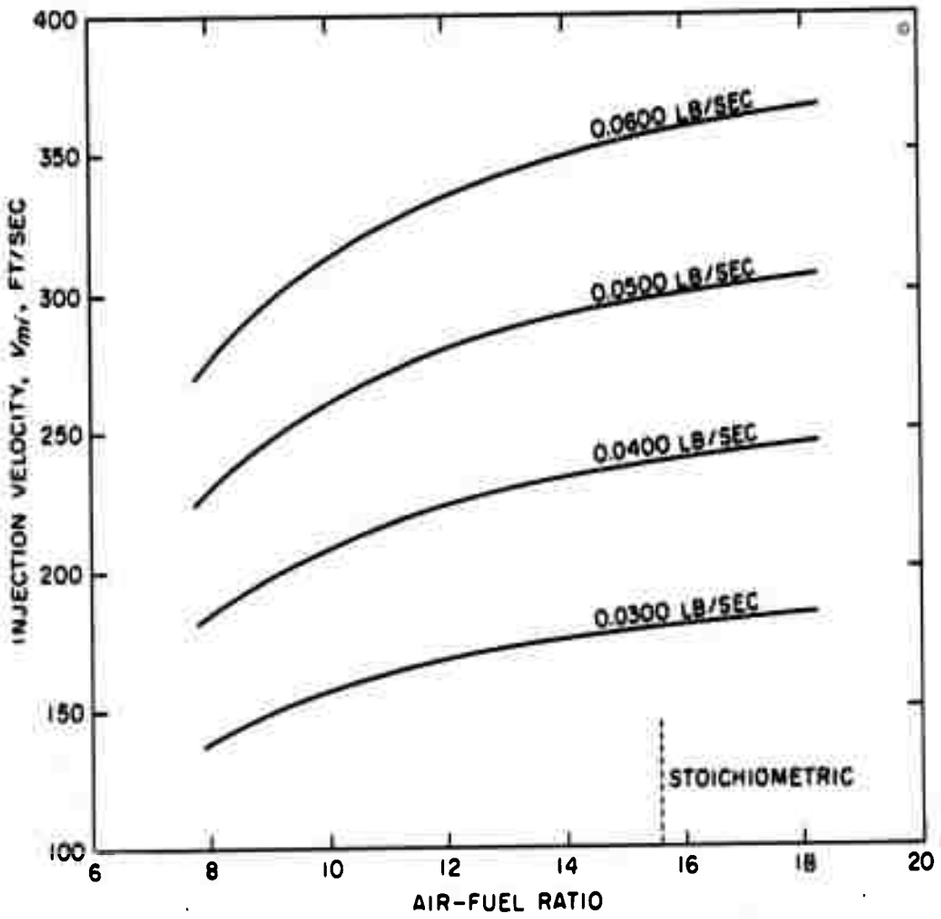

FIG. 4. Theoretical Injection Velocity Versus Air–Fuel Ratio for Various Air Flow Rates.

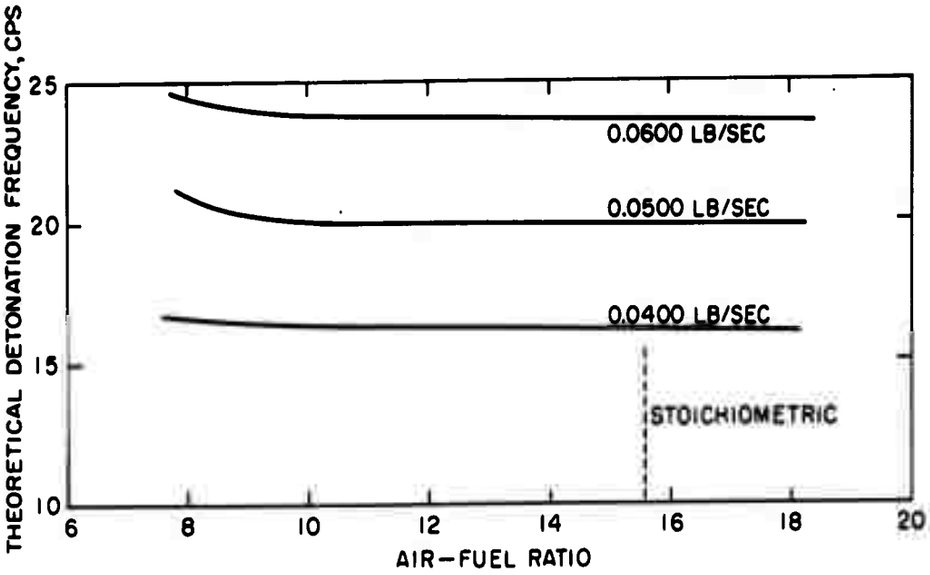

FIG. 5. Theoretical Detonation Frequencies for Various Air Flow Rates.

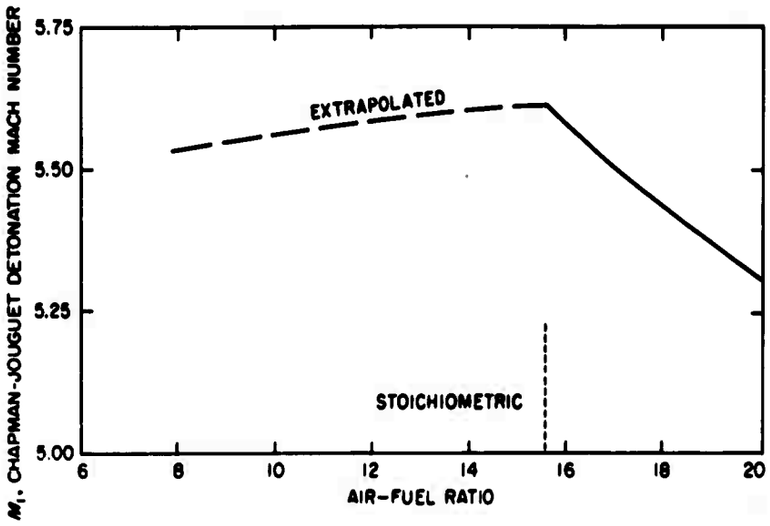

FIG. 6. Chapman-Jouguet Detonation Mach Number as a Function of Air–Fuel Ratio for Propane–Air Mixtures.

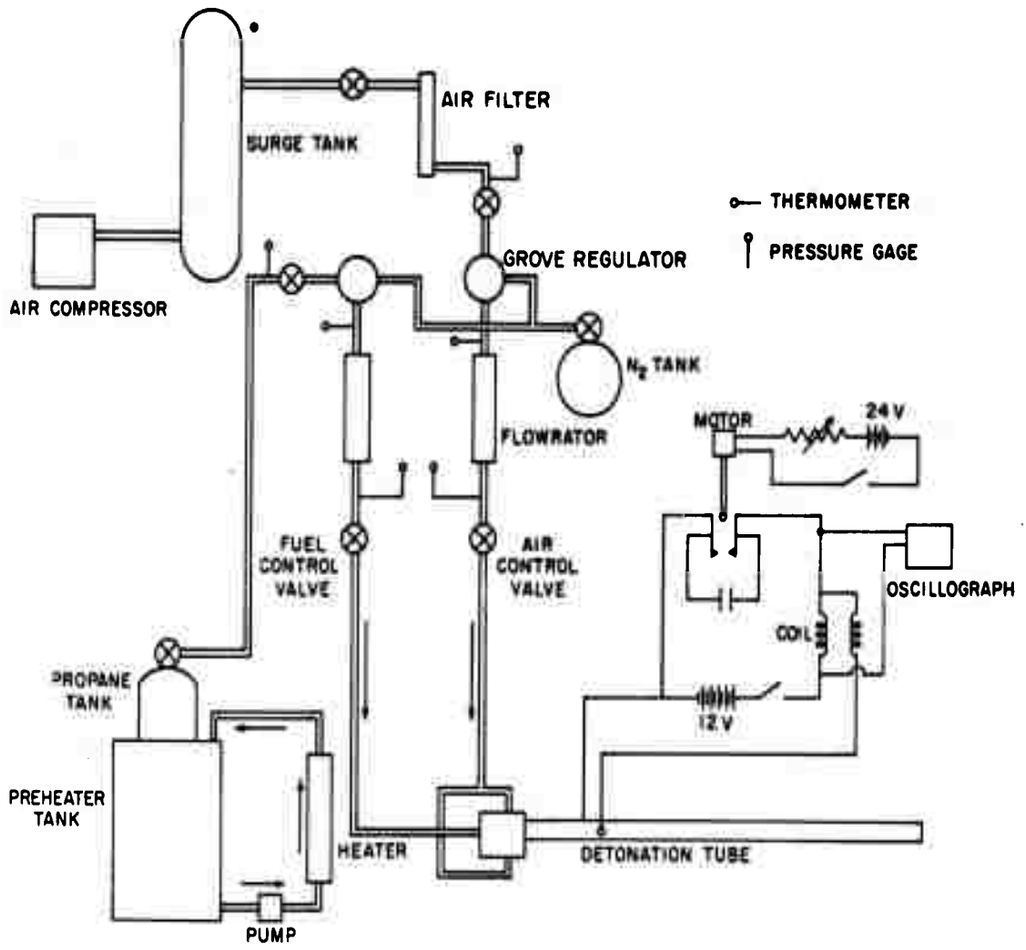

FIG. 7. Flow Diagram.

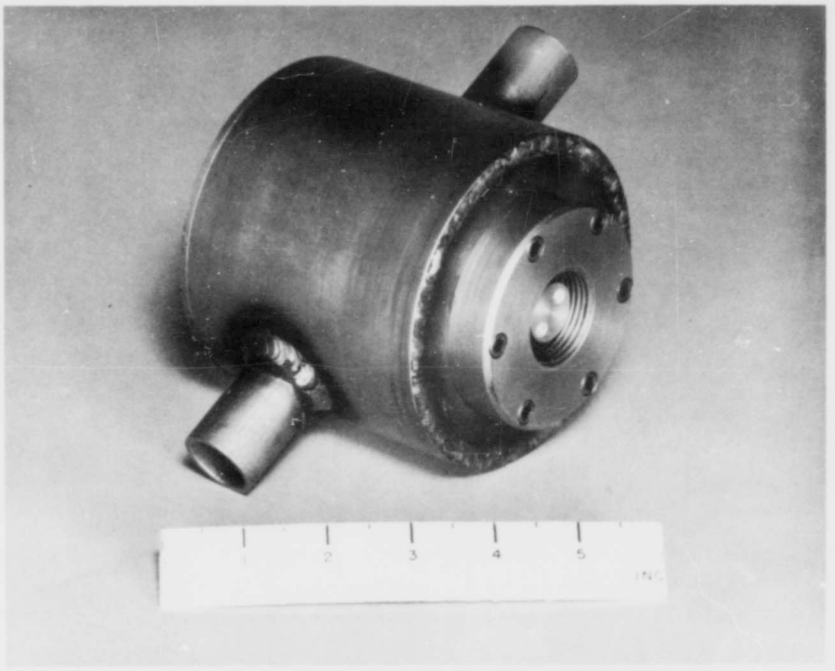

FIG. 8. Air Manifold.

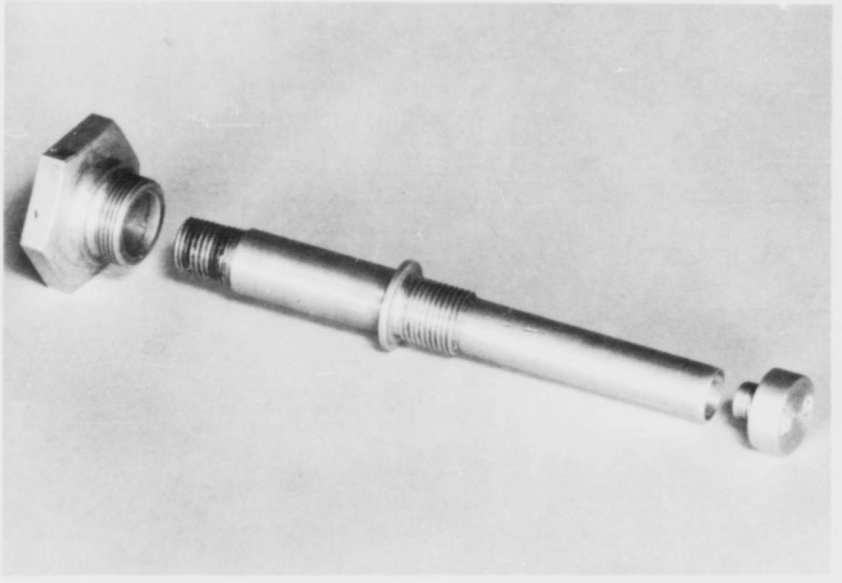

FIG. 9. Fuel Injector.

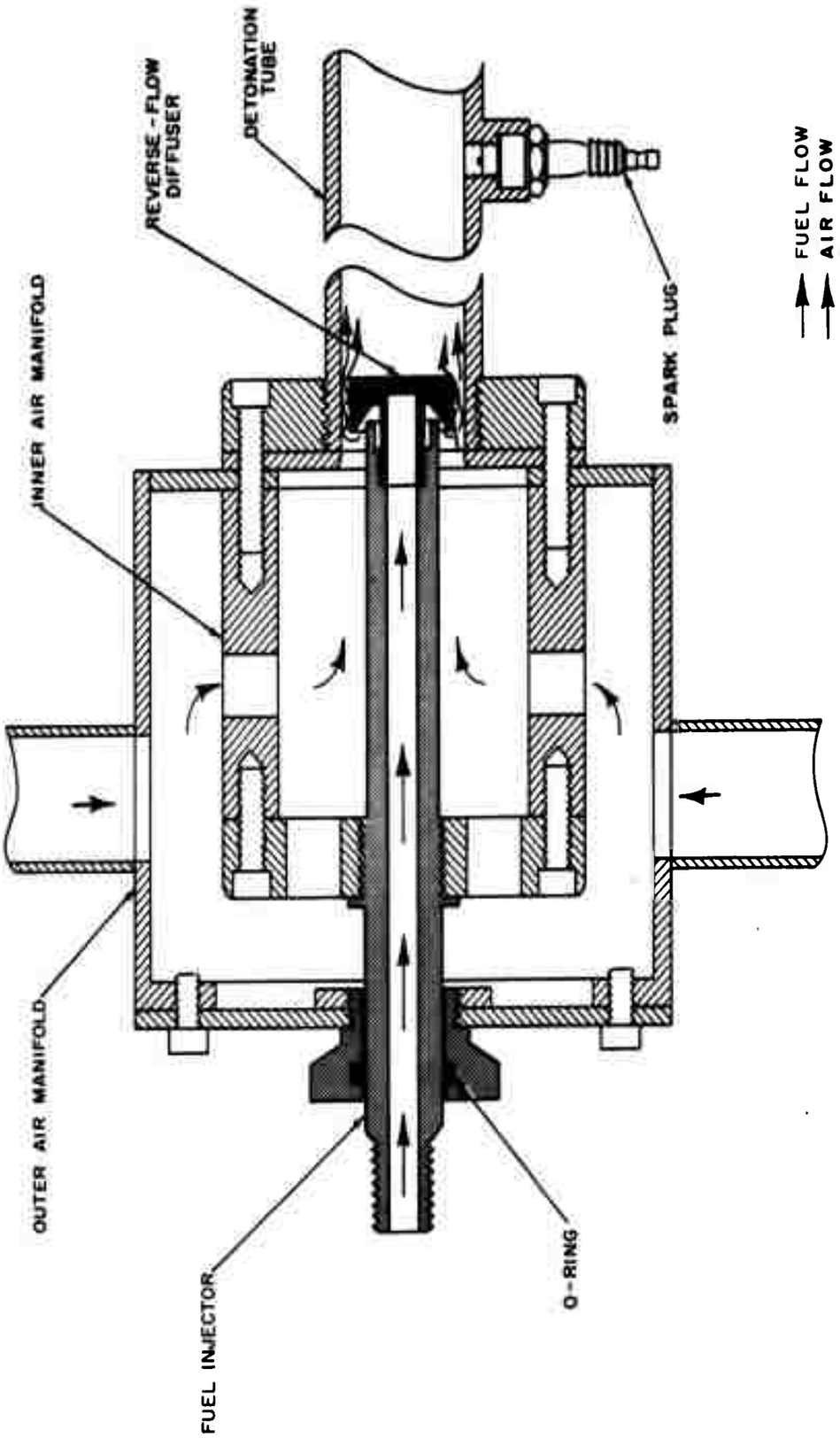

FIG. 10. Air Manifold and Injector Assembly.

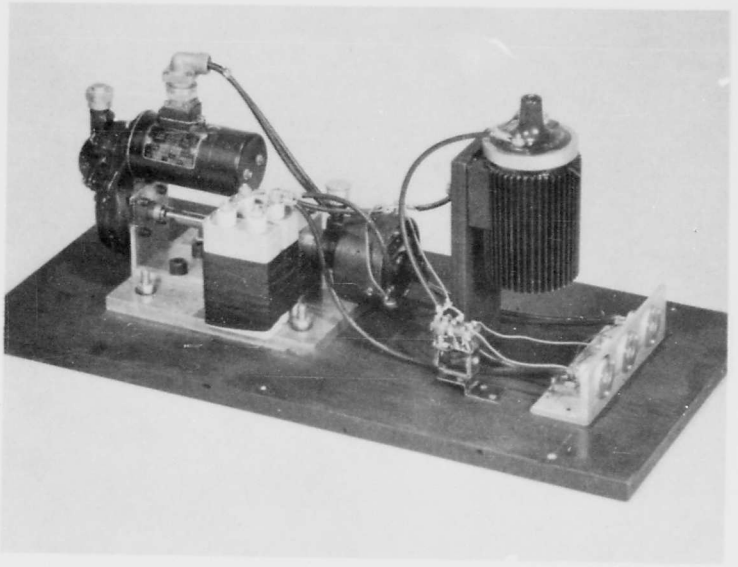

FIG. 11. Variable-Speed Spark Device.

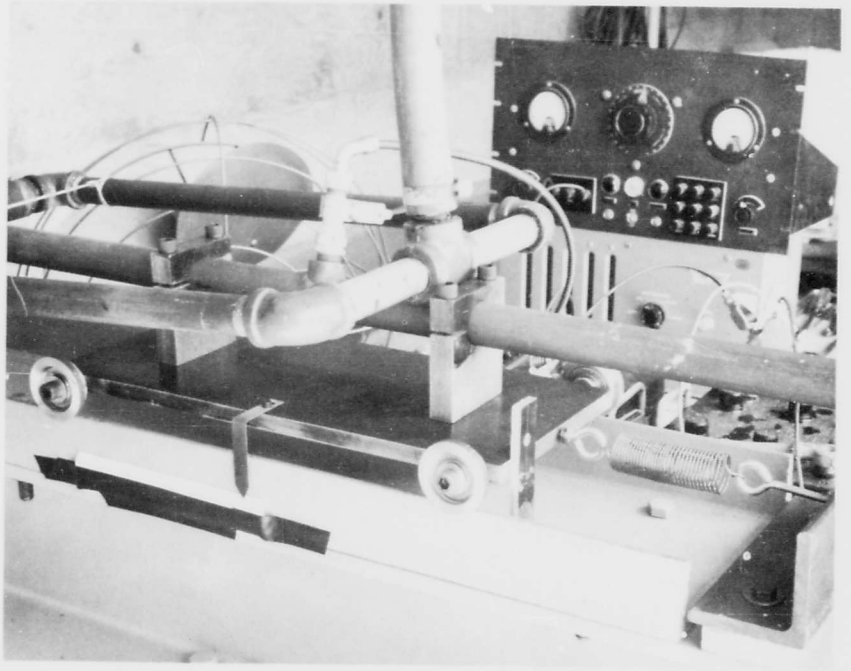

FIG 12. Thrust-Measurement Apparatus.

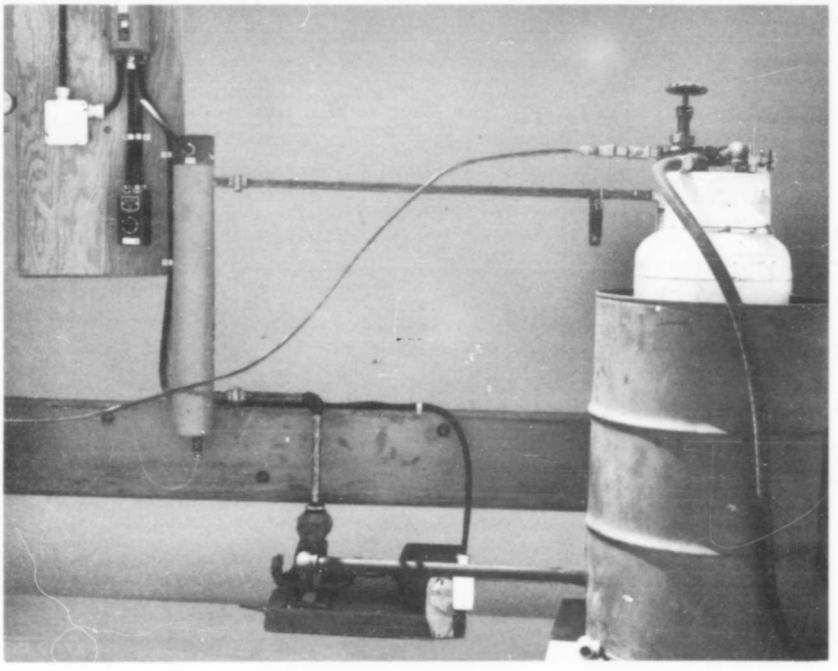

FIG. 13. Propane Supply.

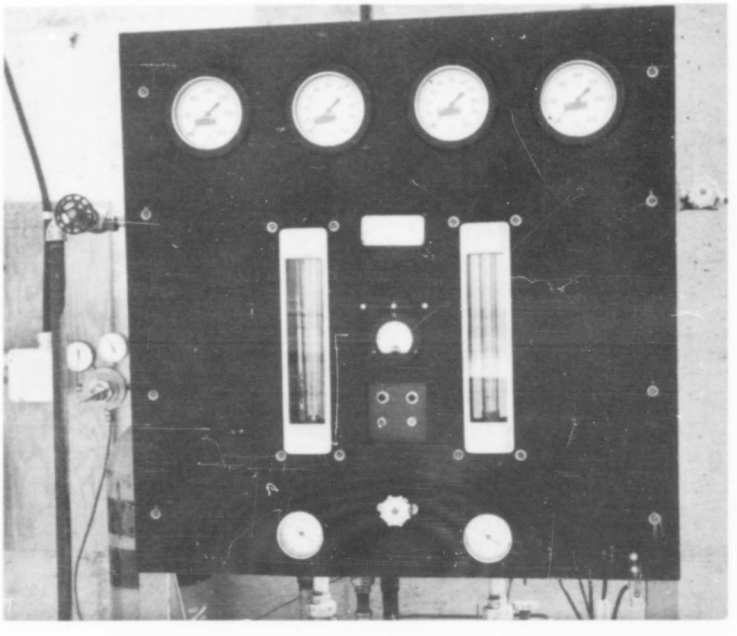

FIG. 14. Control Panel.

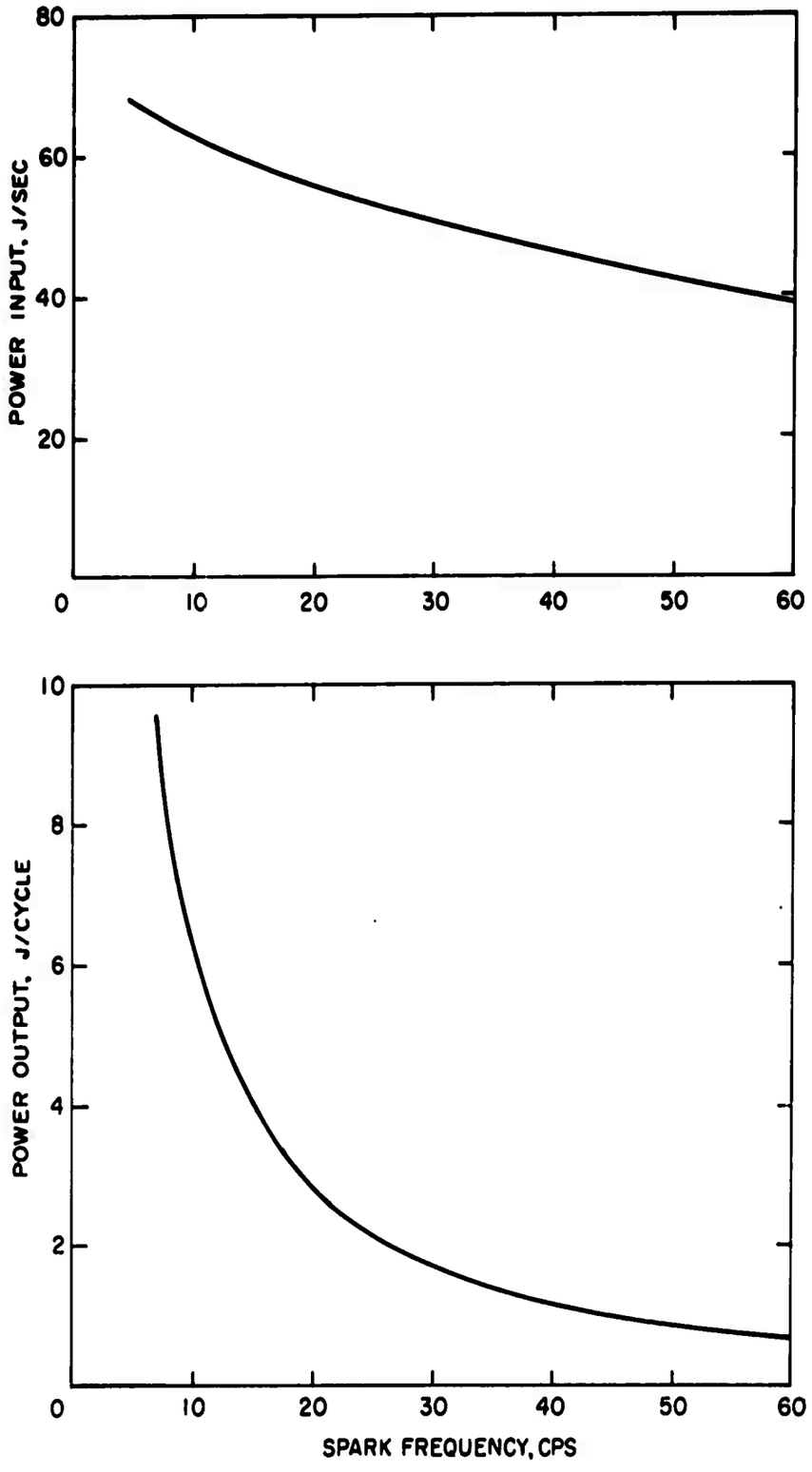

FIG. 15. Ignition-Coil Power Input and Output Versus Frequency of Ignition-Coil Energization.

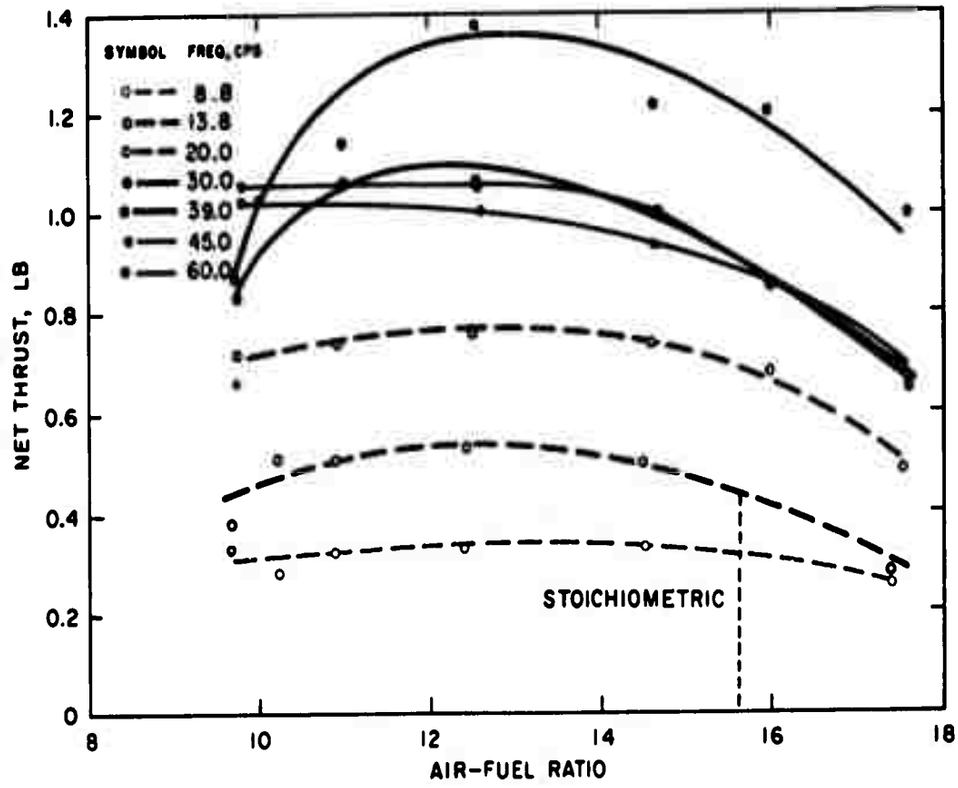

FIG. 16. Net Thrust Versus Air–Fuel Ratio for Air Flow Rate of 0.0400 lb/sec at Various Frequencies.

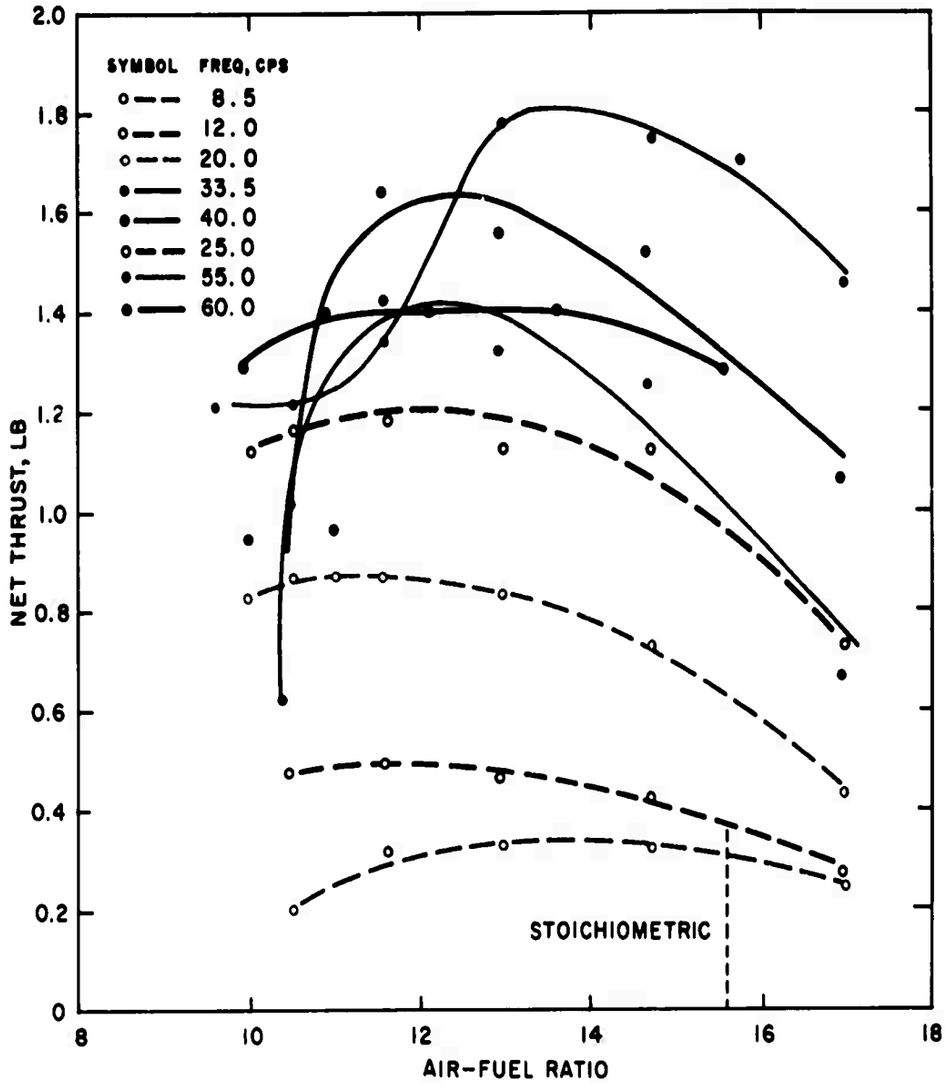

FIG. 17. Net Thrust Versus Air–Fuel Ratio for Air Flow Rate of 0.0500 lb/sec at Various Frequencies.

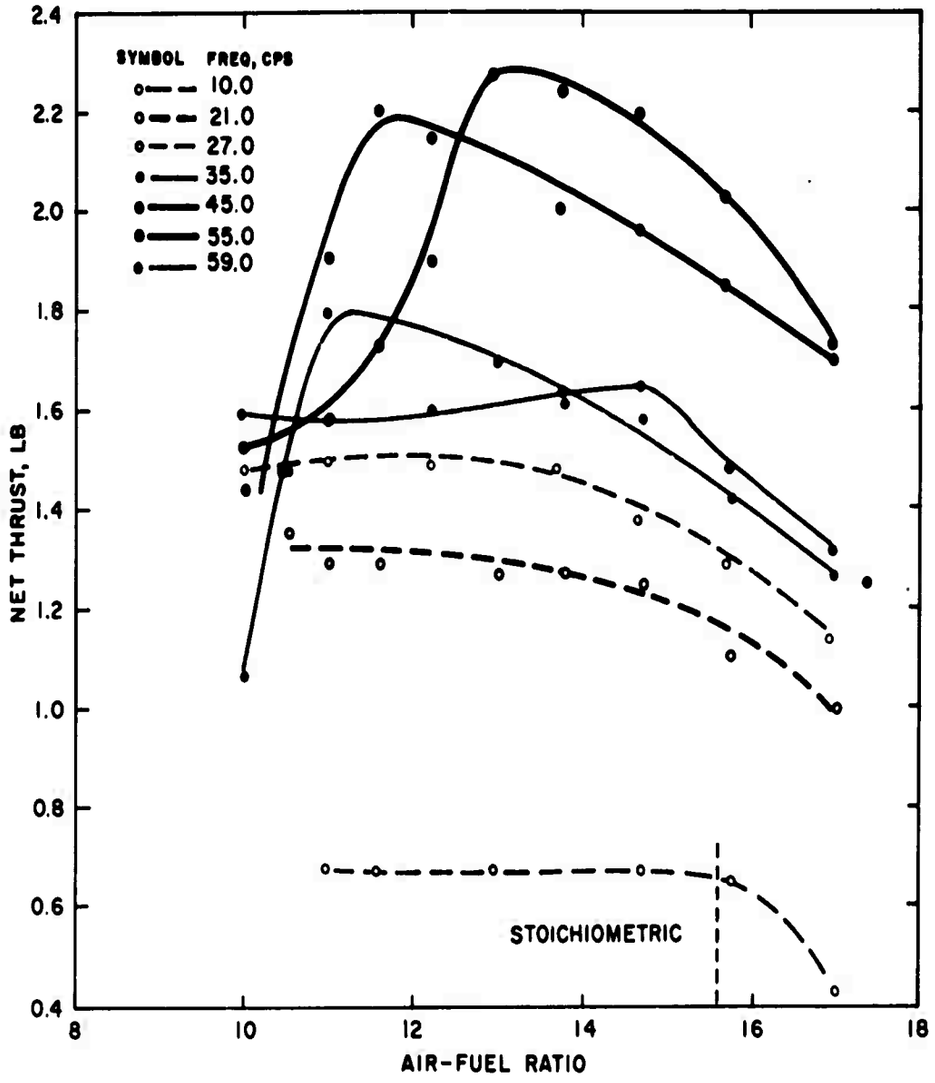

FIG. 18. Net Thrust Versus Air–Fuel Ratio for Air Flow Rate of 0.0576 lb/sec at Various Frequencies.

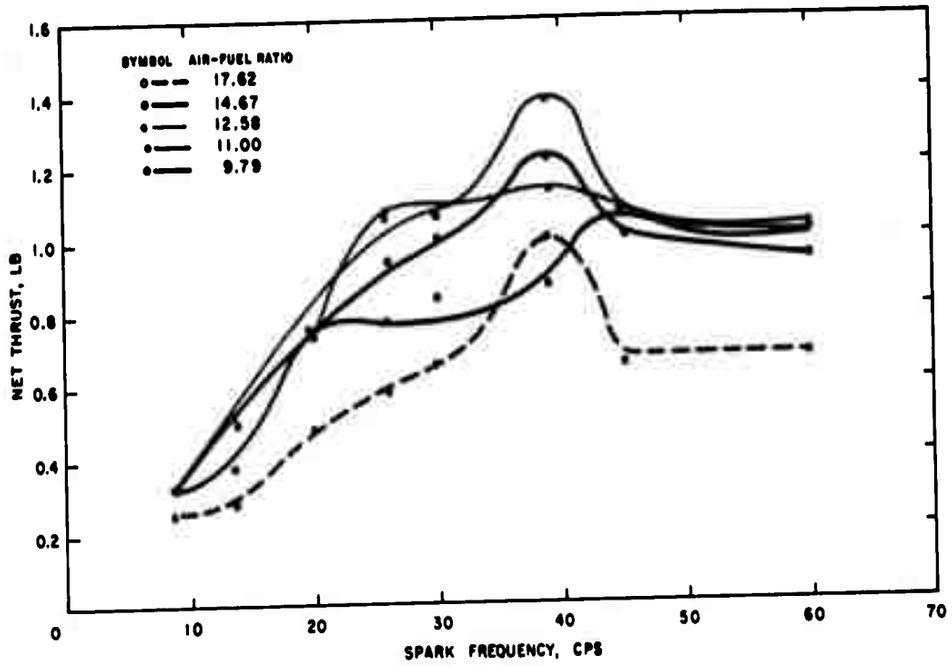

FIG. 19. Net Thrust Versus Spark-Energization Frequency for Air Flow Rate of 0.0400 lb/sec at Various Air–Fuel Ratios.

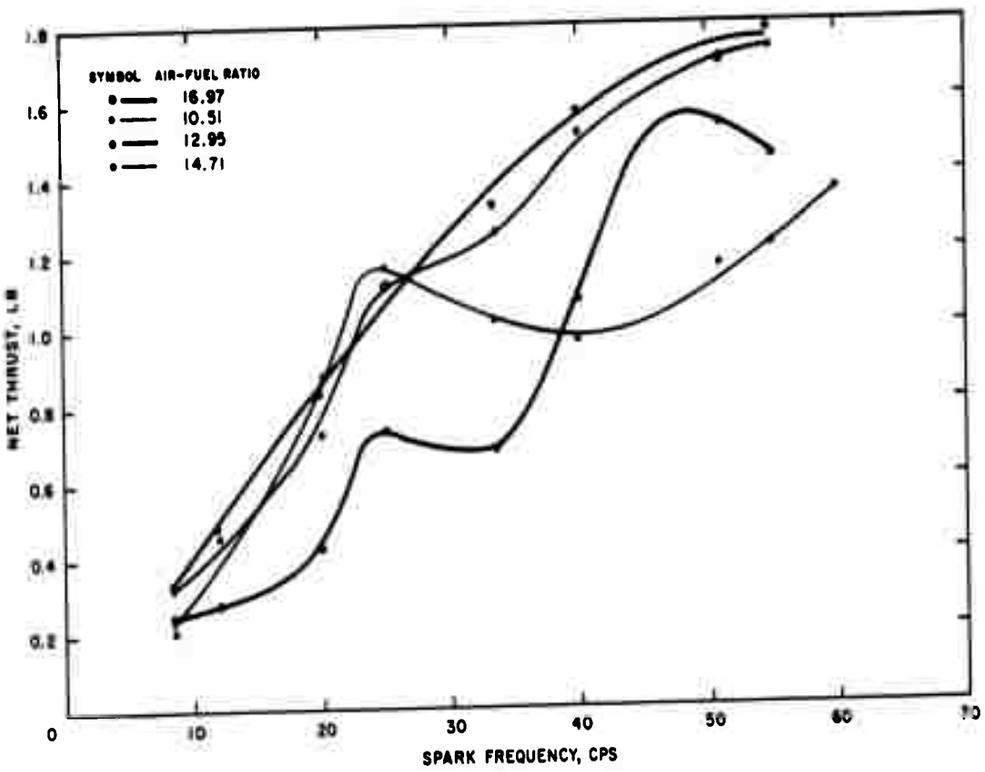

FIG. 20. Net Thrust Versus Spark-Energization Frequency for Air Flow Rate of 0.0500 lb/sec at Various Air–Fuel Ratios.

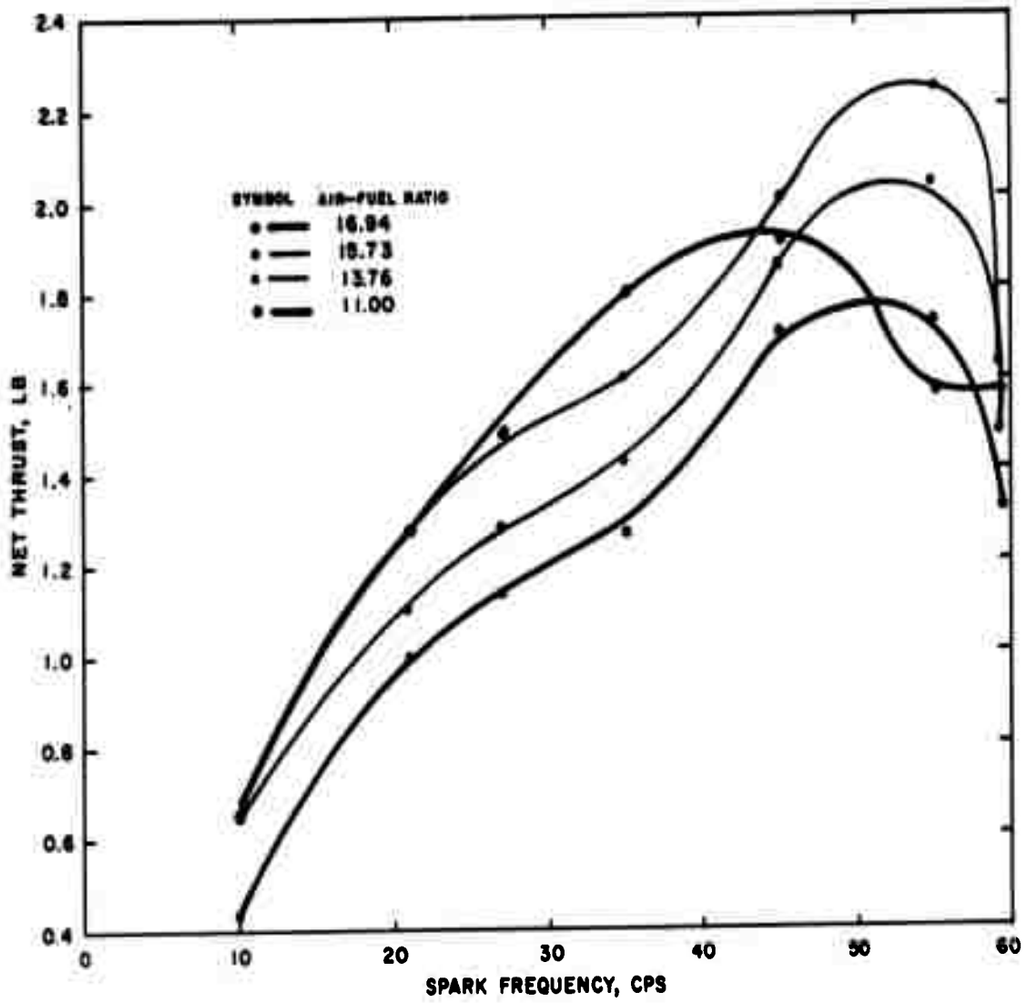

FIG. 21. Net Thrust Versus Spark-Energization Frequency for Air Flow Rate of 0.0576 lb/sec at Various Air–Fuel Ratios.

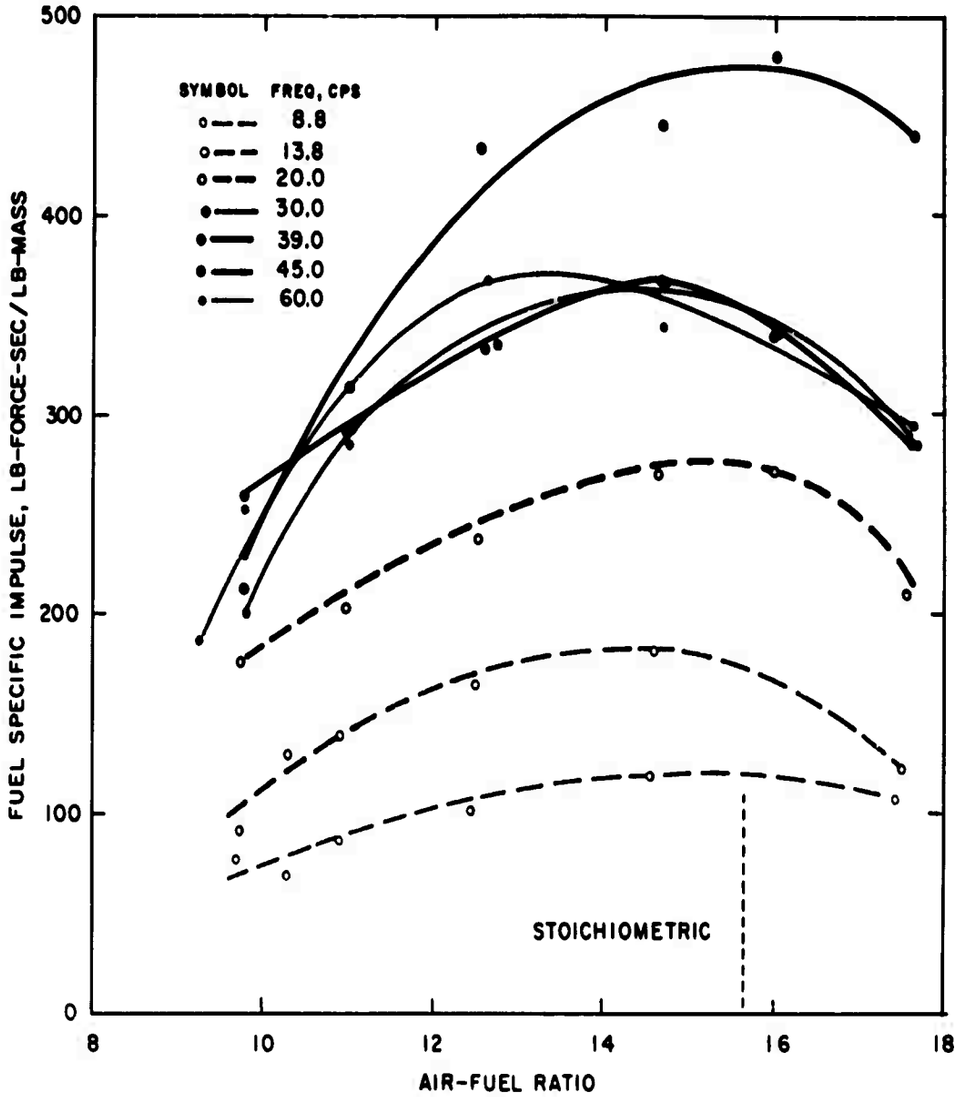

FIG. 22. Fuel Specific Impulse Versus Air–Fuel Ratio for Air Flow Rate of 0.0400 lb/sec at Various Frequencies.

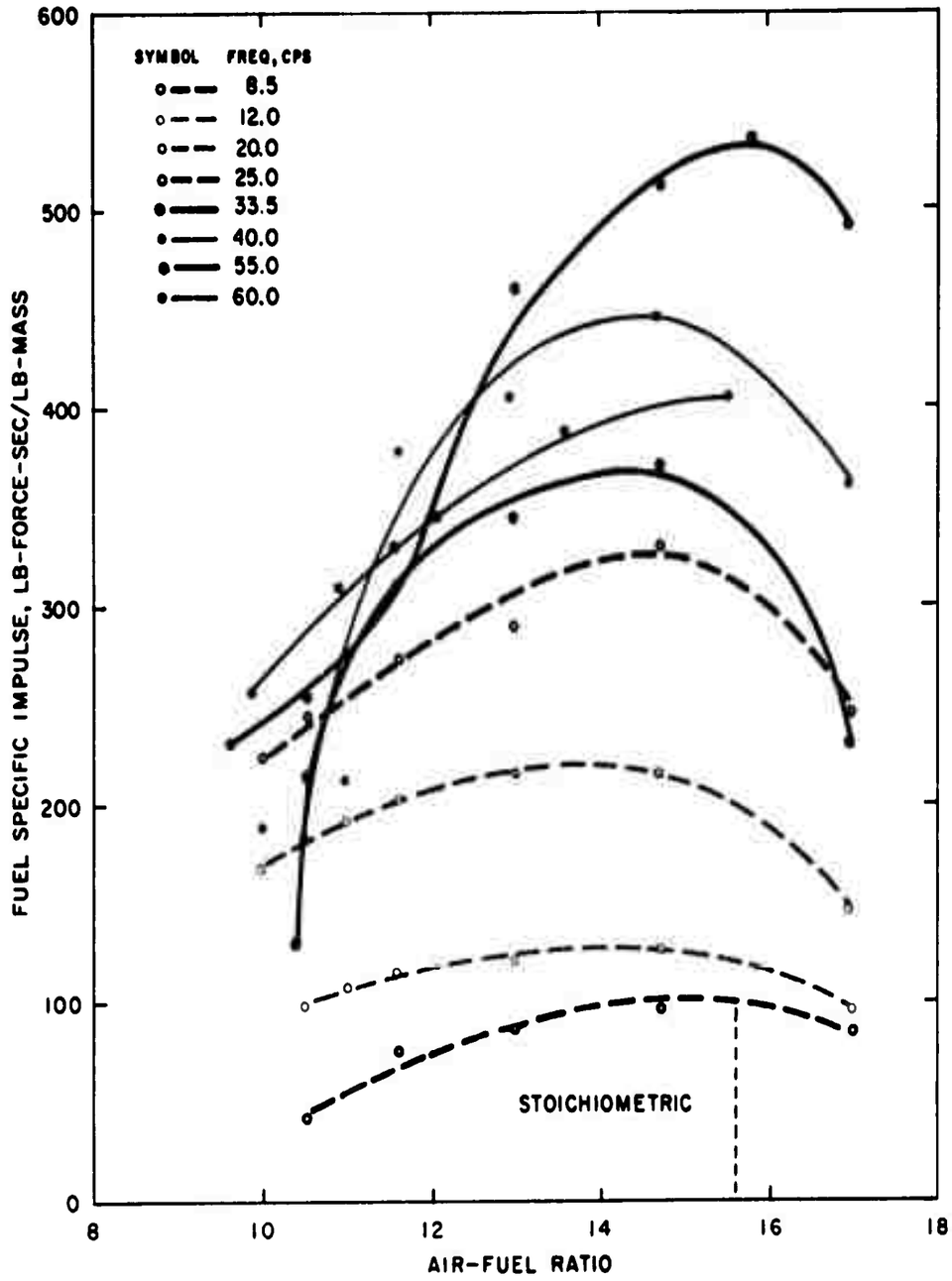

FIG. 23. Fuel Specific Impulse Versus Air–Fuel Ratio for Air Flow Rate of 0.0500 lb/sec at Various Frequencies.

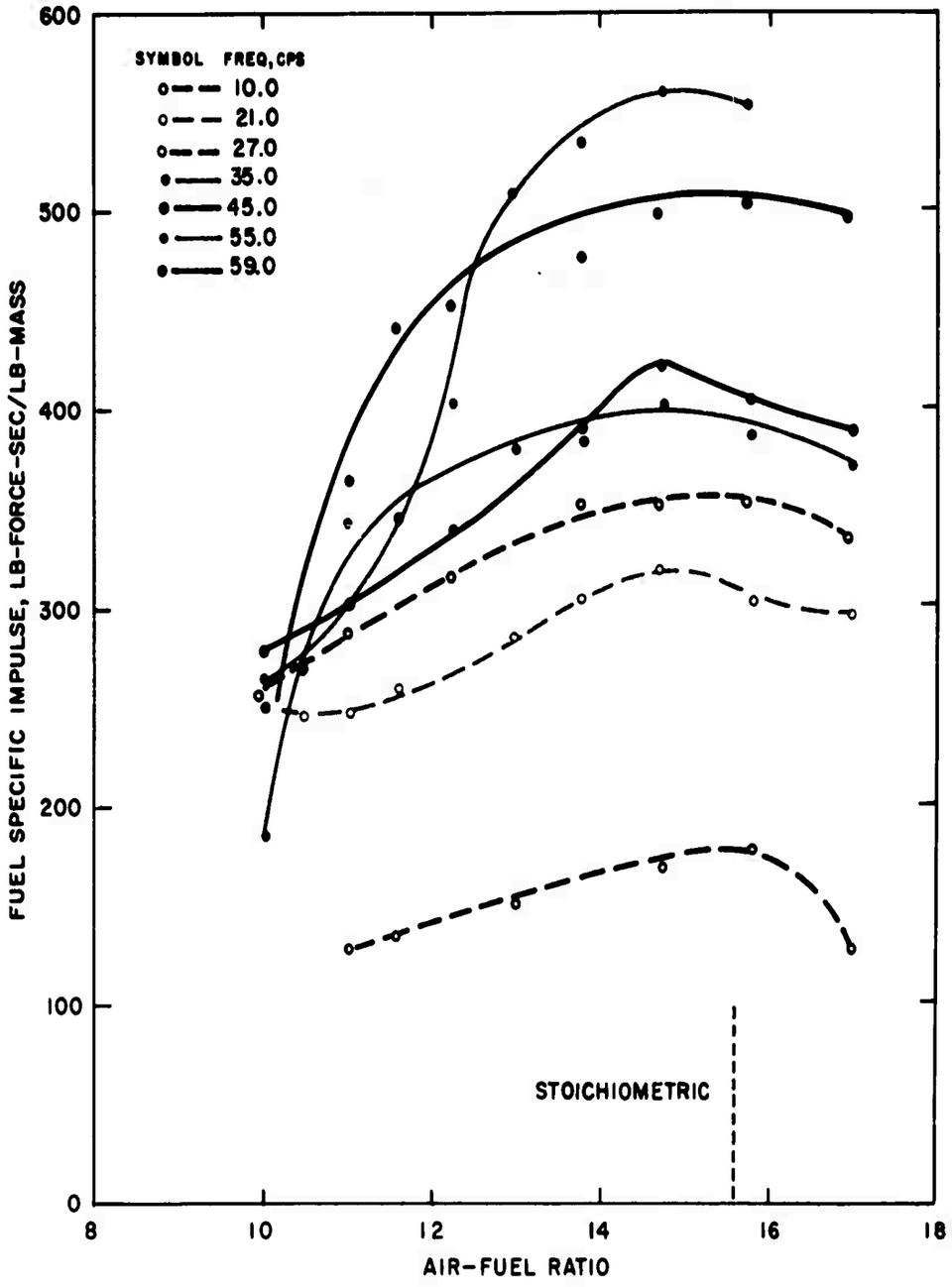

FIG. 24. Fuel Specific Impulse Versus Air–Fuel Ratio for Air Flow Rate of 0.0576 lb/sec at Various Frequencies.

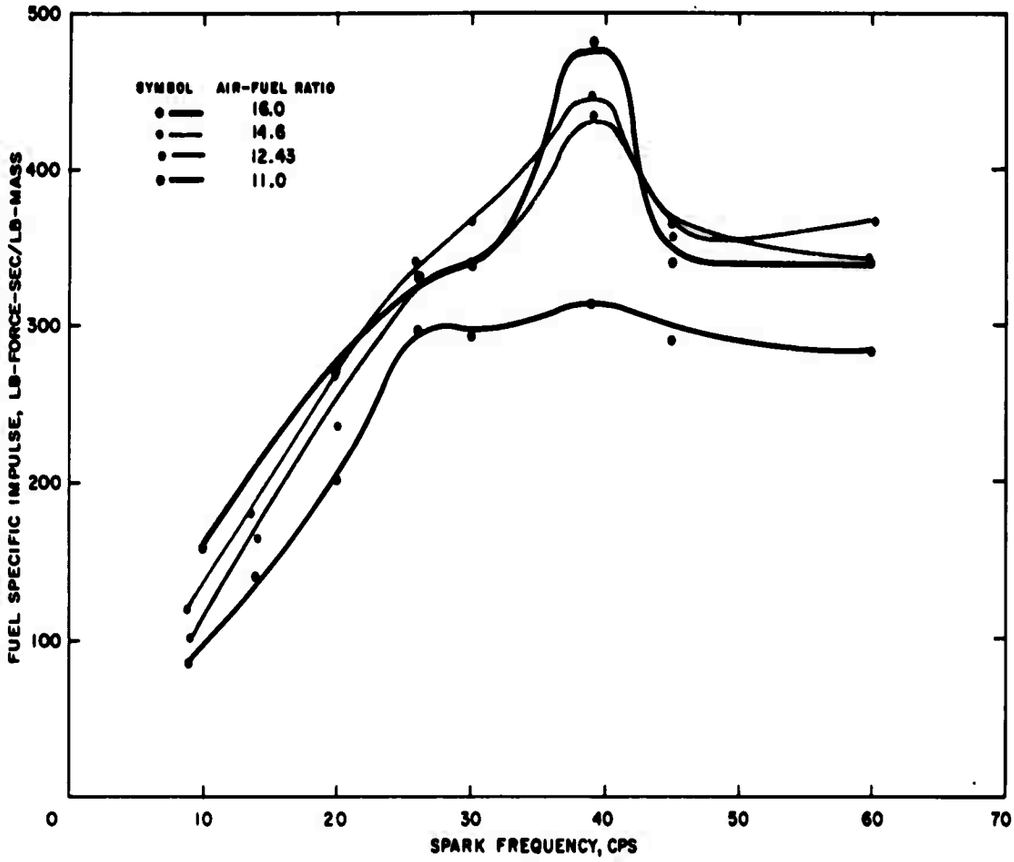

FIG. 25. Fuel Specific Impulse Versus Spark-Energization Frequency for Air Flow Rate of 0.0400 lb/sec at Various Air–Fuel Ratios.

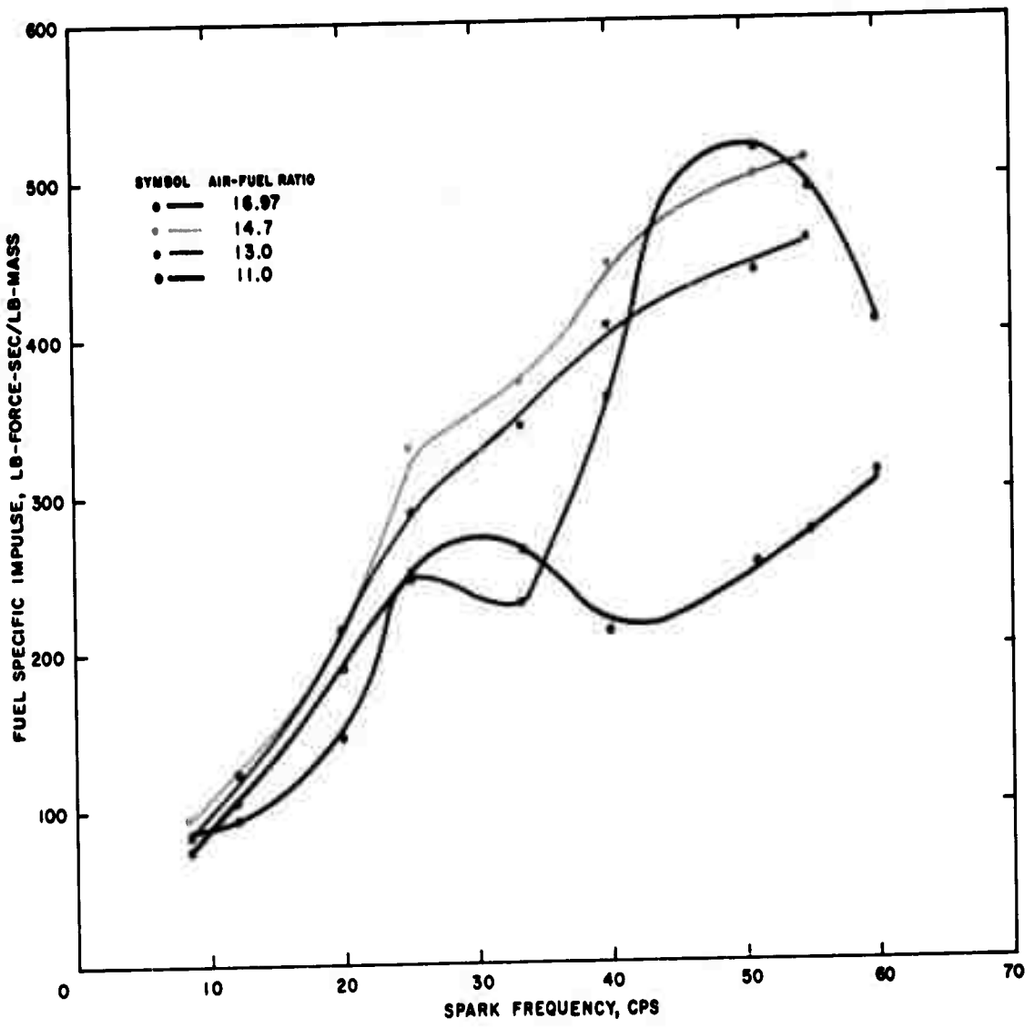

FIG. 26. Fuel Specific Impulse Versus Spark-Energization Frequency for Air Flow Rate of 0.0500 lb/sec at Various Air–Fuel Ratios.

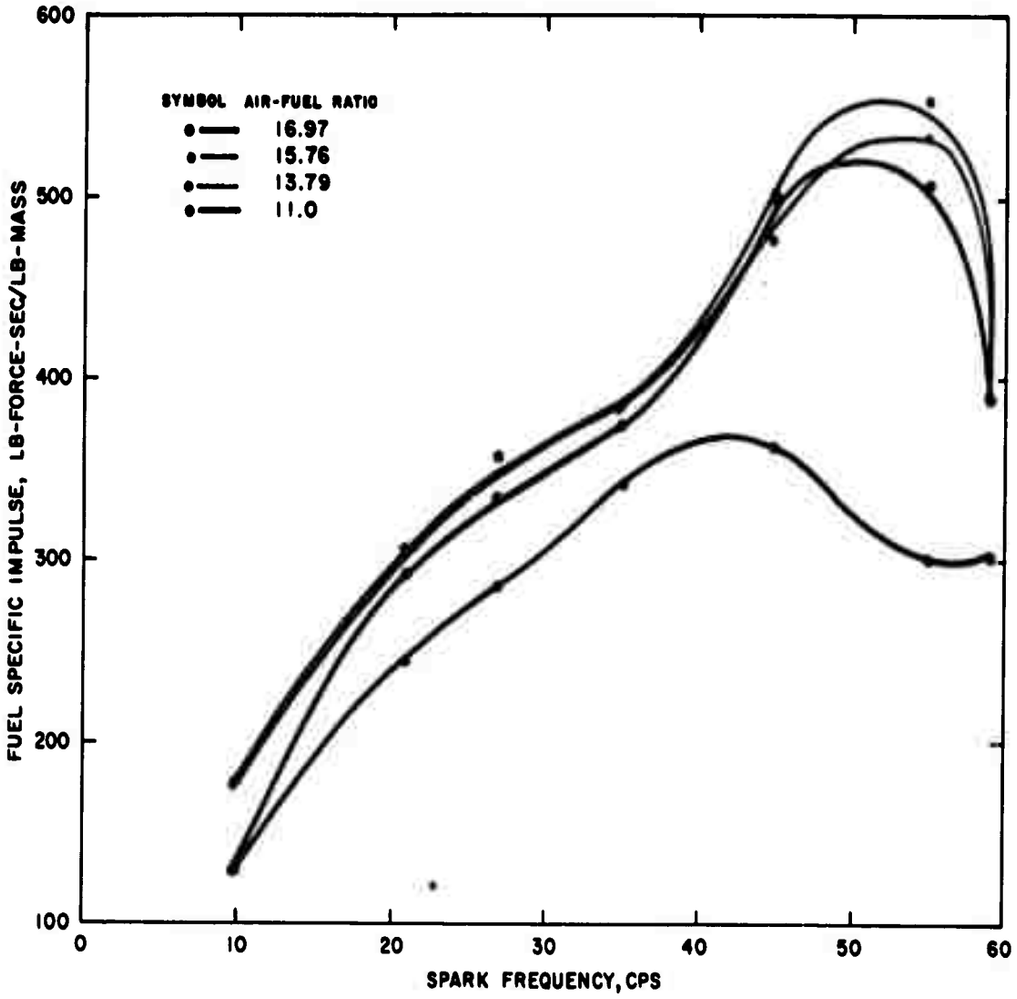

FIG. 27. Fuel Specific Impulse Versus Spark-Energization Frequency for Air Flow Rate of 0.0576 lb/sec at Various Air–Fuel Ratios.

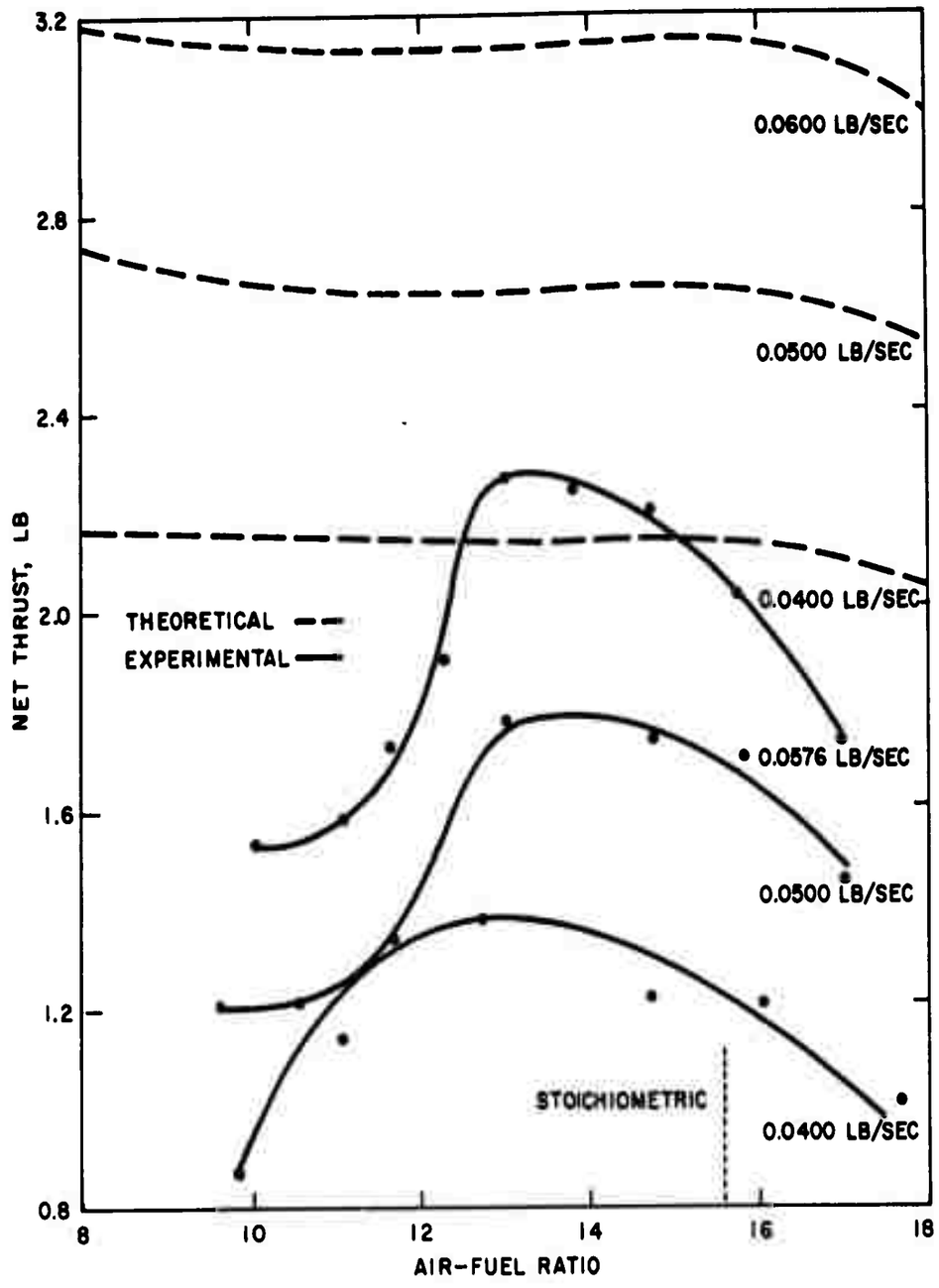

FIG. 28. Comparison of Experimental and Theoretical Maximum Net Thrust for Various Air Flow Rates.

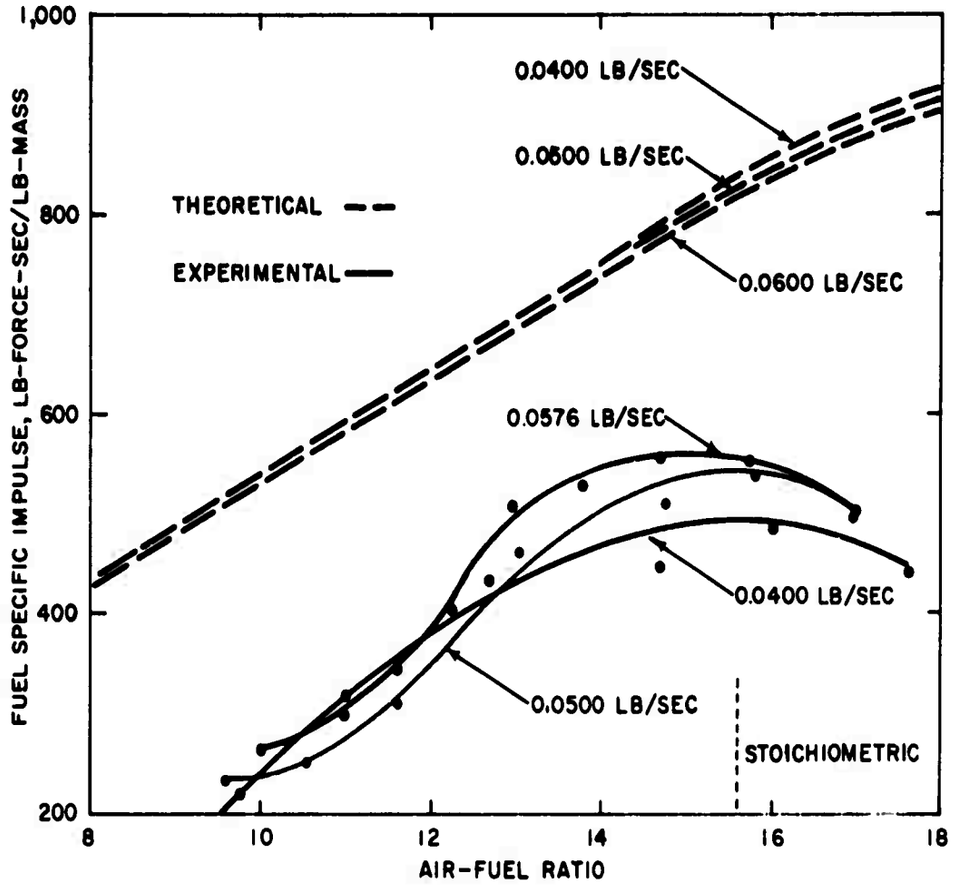

FIG. 29. Comparison of Experimental and Theoretical Maximum Fuel Specific Impulse for Various Air Flow Rates.

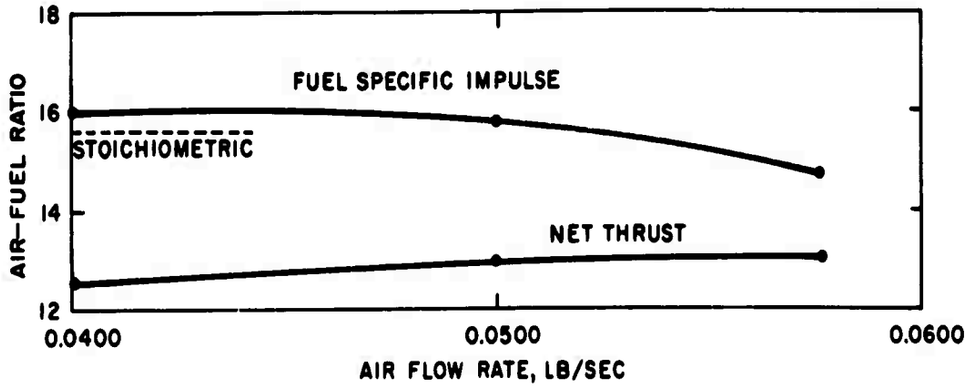

FIG. 30. Maximum Fuel Specific Impulse and Maximum Net Thrust as a Function of Air–Fuel Ratio and Air Flow Rate.

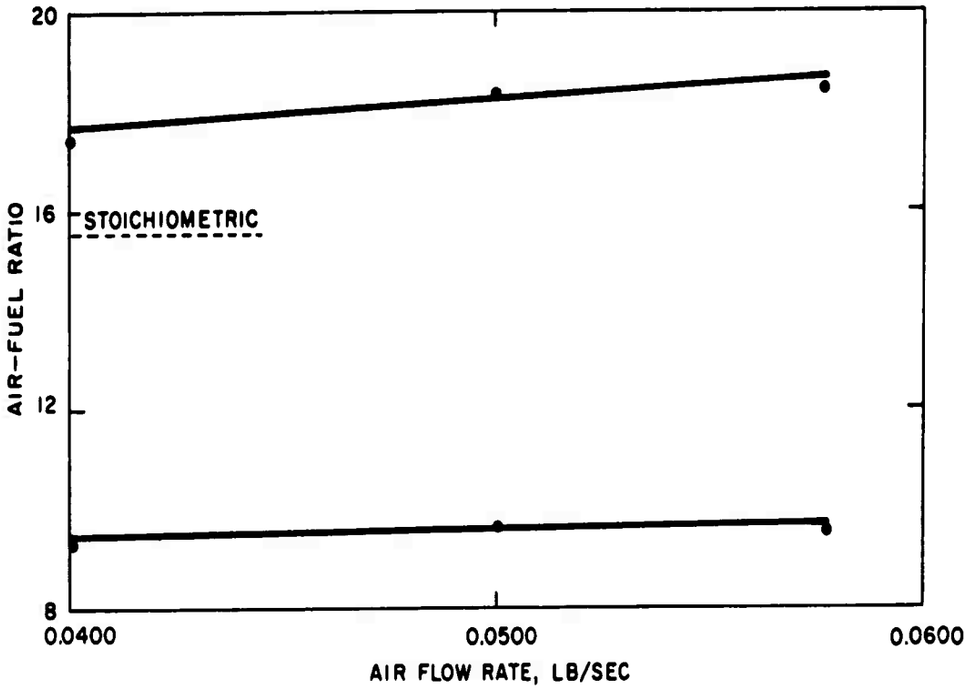

FIG. 31. Experimentally Determined Upper and Lower Limits of Detonability.

REFERENCES

1. Berthelot, M., and Vieille, P. "Sur la Vitesse de Propagation des Phenomenes Explosifs dans les Gas," ACAD SCI (Paris) COMPT REND, Vol. 93 (1881), pp. 18–22.
2. Mallard, E., and LeChatelier, H. "Sur la Vitesse de Propagation de L'inflammation dans les Melanzes Explosifs," ACAD SCI (Paris) COMPT REND, Vol. 93 (18 Juillet 1881), pp. 145–148.
3. Chapman. "On the Rate of Explosions in Gases," PHIL MAG, Vol. 47 (1899), p. 90.
4. Jouguet. "Sur la Propagation des Reactions Chimiques dans les Gaz," J MATH, Ser. 6, Vol. 1 (1905), p. 347; Ser. 6, Vol. 2 (1906), p. 6.
5. Dixon, H. B., ROY SOC LONDON PHIL TRANS, Series A, Vol. 184 (1893), p. 97; Series A, Vol. 200 (1903), p. 315.
6. Von Neumann, J. "Theory of Detonation Waves," Prog. Dept. No. 238 to April 1, 1942 OSRD Rept. No. 549 (1942), Ballistic Research Lab. File No. X-122, Inst. for Adv. Study, May 4, 1942.
7. Doring, W. "Uder den Detonationsvorgang in Gasen," ANN PHYS, Vol. 43 (1943), p. 421.
8. Zeldovitch, Y. G. "Theory of Propagation of Detonations in Gaseous Systems," J EXP THEORET PHYS (USSR), Vol. 10 (1940), p. 542.
9. Greifer, B., and others. "Combustion and Detonation in Gases," J APPL PHYS, Vol. 28, No. 3 (1957), p. 289.
10. Hirschfelder, J. O., and Curtiss, C. F. "Theory of Detonations I," University of Wisconsin, CM-911, NOrd-15884-Series 8, 28 Aug. 1957.
11. Turin, J. J., and Huebler, J. "Advanced Studies in the Combustion of Industrial Gases," American Gas Association, Project IGR-59, April 1951.
12. Shckelkin, K. I. J TECH PHYS USSR, Vol. 17 (1947), p. 613.
13. A Shock Tube Investigation of Detonative Combustion, by R. B. Morrison. Willow Run Research Center, Engineering Research Center, University of Michigan. Ann Arbor, Mich., January 1952. (UMM-97.)
14. British Intelligence. "Reaction-Propulsion Produced by Intermittent Detonative Combustion," by H. Hoffmann. Halstead Exploiting Centre Translation, Research Report No. 1265. British Intelligence, Objectives Sub-Committee Group II, War Office, London, England.
15. Nicholls, J. A., and others. "Intermittent Detonation as a Thrust-Producing Mechanism," AM ROCKET SOC, J, Vol. 27 (1957), pp. 534–41.
16. Rudinger, G. Wave Diagrams for Nonsteady Flow in Ducts. New York, Van Nostrand, 1955.
17. Hall, N. A. Thermodynamics of Fluid Flow. Englewood Cliffs, N. J., Prentice-Hall, Inc., 1957.
18. Eisen, C. L., and others. "Theoretical Calculations in Gaseous Detonation," AFOSR TN 58-326, ASTIA No. AD 154-230, 1958.
19. Lewis, B., and Von Elbe, G. Combustion, Flames and Explosions. New York, Academic Press, 1951.

ABSTRACT CARD

U. S. Naval Ordnance Test Station

Performance Characteristics of an Intermittent-Detonation Device, by L. J. Krzycki. China Lake, Calif., NOTS, July 1962. 48 pp. (NAVWEPS Report 7655, NOTS TP 2680), UNCLASSIFIED.

ABSTRACT. An analytical and experimental investigation was conducted to determine the operating characteristics of an intermittent-combustion device employing gaseous detonative combustion. Gaseous propane and air were used as propellants in the experimental investigation.

Results indicated that the intermittent-detonation device was capa-

(Over)

1 card, 4 copies

U. S. Naval Ordnance Test Station

Performance Characteristics of an Intermittent-Detonation Device, by L. J. Krzycki. China Lake, Calif., NOTS, July 1962. 48 pp. (NAVWEPS Report 7655, NOTS TP 2680), UNCLASSIFIED.

ABSTRACT. An analytical and experimental investigation was conducted to determine the operating characteristics of an intermittent-combustion device employing gaseous detonative combustion. Gaseous propane and air were used as propellants in the experimental investigation.

Results indicated that the intermittent-detonation device was capa-

(Over)

1 card, 4 copies

U. S. Naval Ordnance Test Station

Performance Characteristics of an Intermittent-Detonation Device, by L. J. Krzycki. China Lake, Calif., NOTS, July 1962. 48 pp. (NAVWEPS Report 7655. NOTS TP 2680), UNCLASSIFIED.

ABSTRACT. An analytical and experimental investigation was conducted to determine the operating characteristics of an intermittent-combustion device employing gaseous detonative combustion. Gaseous propane and air were used as propellants in the experimental investigation.

Results indicated that the intermittent-detonation device was capa-

(Over)

1 card, 4 copies

U. S. Naval Ordnance Test Station

Performance Characteristics of an Intermittent-Detonation Device, by L. J. Krzycki. China Lake, Calif., NOTS, July 1962. 48 pp. (NAVWEPS Report 7655. NOTS TP 2680), UNCLASSIFIED.

ABSTRACT. An analytical and experimental investigation was conducted to determine the operating characteristics of an intermittent-combustion device employing gaseous detonative combustion. Gaseous propane and air were used as propellants in the experimental investigation.

Results indicated that the intermittent-detonation device was capa-

(Over)

1 card, 4 copies

ble of operating on at least two "resonant" spark-energization frequencies. For the device used in the investigation these frequencies were approximately 25 and 50 cps. Reaction thrust, noise output, and actual combustion frequency were noticeably greater at the resonant conditions than at other operating points.

Reloading the tube with fresh charge occupied most of the cycle time, which limits the operating frequency of the device. The device does not appear promising as a thrust producing mechanism because of its low operating frequencies.

NAVWEPS Report 7655

ble of operating on at least two "resonant" spark-energization frequencies. For the device used in the investigation these frequencies were approximately 25 and 50 cps. Reaction thrust, noise output, and actual combustion frequency were noticeably greater at the resonant conditions than at other operating points.

Reloading the tube with fresh charge occupied most of the cycle time, which limits the operating frequency of the device. The device does not appear promising as a thrust producing mechanism because of its low operating frequencies.

NAVWEPS Report 7655

ble of operating on at least two "resonant" spark-energization frequencies. For the device used in the investigation these frequencies were approximately 25 and 50 cps. Reaction thrust, noise output, and actual combustion frequency were noticeably greater at the resonant conditions than at other operating points.

Reloading the tube with fresh charge occupied most of the cycle time, which limits the operating frequency of the device. The device does not appear promising as a thrust producing mechanism because of its low operating frequencies.

NAVWEPS Report 7655

ble of operating on at least two "resonant" spark-energization frequencies. For the device used in the investigation these frequencies were approximately 25 and 50 cps. Reaction thrust, noise output, and actual combustion frequency were noticeably greater at the resonant conditions than at other operating points.

Reloading the tube with fresh charge occupied most of the cycle time, which limits the operating frequency of the device. The device does not appear promising as a thrust producing mechanism because of its low operating frequencies.

UNCLASSIFIED